APPLICATION OF PHOTON CORRELATION SPECTROSCOPY TO FLOWING BROWNIAN MOTION SYSTEMS

by

DALIA P. CHOWDHURY

B.S. Bangladesh University of Engineering and Technology, 1979

A MASTER'S THESIS

Submitted in partial fulfillment of
the requirements for the degree

MASTER OF SCIENCE

College of Engineering

Department of Nuclear Engineering

KANSAS STATE UNIVERSITY

Manhattan, Kansas
1985

Christopher M. Sorensen
Major Professor

TABLE OF CONTENTS

LIST OF FIGURES

LIST OF TABLES

1.0. INTRODUCTION

Flowing Brownian motion systems are encountered in many practical situations of interest e.g., soot particles in flames as well as other aerosol systems. Recently, the dynamic light scattering technique, Photon Correlation Spectroscopy (PCS) has proven useful for studying the diffusional processes in these aerosol systems as well as sizing the aerosol particulates. This has stimulated the need for an understanding of the PCS spectrum of such diffusing and flowing systems. A representative system of such a situation is polystyrene latex spheres suspended in water flowing through a tube at a known flow rate. This system is quite simple to allow for verification of the theoretical spectrum and to establish an experimental basis for the more complicated cases of interest. The purpose of this thesis is to develop a theoretical expression for the PCS spectrum of a system of diffusing and flowing particles and to test this theory with this well characterized system of latex spheres in water.

The diffusive motion of a system of particles may be investigated by studying the spectrum of initially monochromatic light scattered by the particles. If the incident light source is a laser, and the scattered light falls on the photosurface of a photomultiplier tube, then by measuring the spectrum of the photocurrent one obtains the spectrum of the intensity fluctuations of the scattered light. The intensity of the scattered light is determined by the instantaneous superposition of the phases of the waves scattered from each of the diffusing particles. The intensity fluctuates because the particles move. By finding the correlation function of the scattered light, we can estimate the particle

size, or if the particle size is known, if needed we can calculate the temperature or viscosity. If there exists a bulk motion of the particles relative to the scattering volume, an additional fluctuation is generated in the scattered light. This extra term in the correlation function becomes important only when the correlation time due to the movement of the particles in and out of the sample volume becomes comparable to the time due to the diffusion of the particles.

Two terms 1) the correlation time, τ_1, and 2) the beam transit time, τ_2, are useful in describing a system of particles which are diffusing while in bulk motion. PCS can measure these times. In this thesis, correlation functions for both static and flowing systems are derived for comparison with experiment. The correlation time, τ_1, is due to the random Brownian diffusion of the particles while the beam transit term, τ_2, arises due to the bulk motion of the particles with respect to the scattering volume. The diffusional term appears as an exponential and the beam transit term appears as a Gaussian in the correlation spectrum.

In summary, this thesis presents a theoretical and experimental study of the photon correlation spectrum observed for light scattered from a flowing Brownian motion system. The simple polystyrene-water system as mentioned earlier, was used. The study of the simple system allowed us to study the effect of both the diffusion and the flow terms in the PCS spectrum and provided a testing ground for our theoretical understanding of the spectrum and the experimental technique. The theory was worked out and was tested with the simple system. It was found that the theory works for such a system. Furthermore, a very useful method of analysis was developed. Finally, it was found that τ_1 and τ_2 could be separated for different flow rates even when τ_2 was much faster than τ_1, a result not previously expected.

2.0 THEORY DEVELOPMENT

2.1 Light Scattering Theory

In the classical theory of light scattering an incident electromagnetic field exerts a force on the charges in the scattering volume. These accelerating charges then radiate light. The incident field is said to polarize the medium. When visible light is incident on the medium, the atoms in a subregion of the illuminated volume, small compared to the cube of the incident light wavelength, see essentially the same incident electric field. If many subregions of equal size are considered, the scattered electric field is the superposition of the scattered fields from each of them. If the subregions are optically identical, that is, each has the same dielectric constant, there will be no scattered light in other than the forward direction. This is so because the wavelets scattered from each subregion are identical except for a phase factor that depends on the relative positions of the subregions. If we ignore surface effects it is clear that for a large medium, each subregion can always be paired with another subregion whose scattered field is identical in amplitude but opposite in phase and will thus cancel, leaving no net scattered field in other than the forward direction. If, however, the regions are optically different, that is, have different dielectric constants, then the amplitudes of the light scattered from the different subregions are no longer identical. Complete cancellation will no longer take place, and there will be scattered light in other than the forward direction. Thus, in this semimacroscopic view, originally introduced by Einstein, light scattering is a result of local fluctuations in the dielectric constant of the medium. Kinetic theory makes it clear that molecules are constantly

translating and rotating so that the instantaneous dielectric constant of a given subregion will fluctuate and thus give rise to light scattering.

Let's consider a nonmagnetic, nonconducting, nonabsorbing medium with average dielectric constant ε_o and refractive index $n = \sqrt{\varepsilon_o}$. Let the incident electric field be a plane wave of the form

$$\vec{E}_i(\vec{r},t) = \hat{\eta}_i E_o \exp i(\vec{k}_i \cdot \vec{r} - \omega_i t)$$

where $\hat{\eta}_i$ is a unit vector in the direction of the incident electric field, E_o is the field amplitude, $\vec{K}_i$ is the wave vector, and ω_i is the angular frequency. This plane wave is incident upon a medium that has a local dielectric constant

$$\vec{\varepsilon}(\vec{r},t) = \varepsilon_o \vec{I} + \partial\vec{\varepsilon}(\vec{r},t)$$

where $\partial\vec{\varepsilon}(r,t)$ is the dielectric constant fluctuation tensor at position $\vec{r}$ and time t and $\vec{I}$ is the second rank unit tensor. The component of the scattered electric field at large distance $\vec{R}$ from the scattering volume with polarization $\hat{\eta}_f$, wave vector $\vec{K}_f$ and frequency ω_f is

$$\vec{E}_s(\vec{R},t) = \frac{E_o}{4\pi R\varepsilon_o} \exp(i \vec{K}_f \cdot \vec{R}) \int_{V_{Scat}} d^3r \exp i(\vec{q}\cdot\vec{r} - i\omega_i t)[\hat{\eta}_f \cdot [\vec{K}_f x (\vec{K}_f x (\partial\vec{\varepsilon}(r,t)\ \hat{\eta}_i)]$$

where the subscript V_{Scat} indicates that the integral is over the scattering volume. The vector $\vec{q}$ is defined in terms of the scattering geometry as

$$\vec{q} = \vec{K}_i - \vec{K}_f$$

Where $\vec{K}_i$ and $\vec{K}_f$ point, respectively, in the direction of propagation of the incident wave and the wave that reaches the detector, respectively. The angle between $\vec{K}_i$ and $\vec{K}_f$ is called the scattering angle θ.

Fig. 2.1.1. The total radiated field at the detector is the superposition of the fields radiated from all infinitesimal volumes d^3r at position $\vec{r}$ with respect to the center of the illuminated volume V. The detector is at position $\vec{R}$ with respect to the center of the illuminated volume.

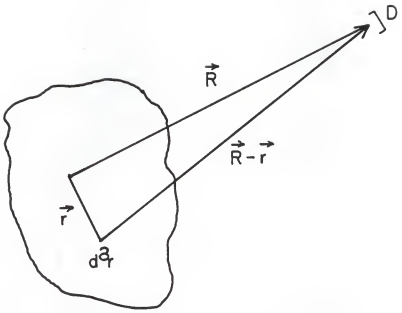
D
$\vec{R}$
$\vec{R}-\vec{r}$
$\vec{r}$
$d\mathcal{B}_r$

Fig. 2.1.2. Light of polarization $\hat{n}_i$ and wave vector $\vec{K}_i$ is scattered in all directions. Only scattered light of wave vector $\vec{K}_f$ and polarization $\hat{n}_f$ arrives at the dtector. The scattering vector $\vec{q} = \vec{K}_i - \vec{K}_f$ is defined by the geometry. Since for elastic scattering the scattered wave has essentially the same wave length as the incident wave, $K_f \cong 2\pi n/\lambda_i = K_i$, it follows from the law of cosines, $q = 2K_i \sin\theta/2$.

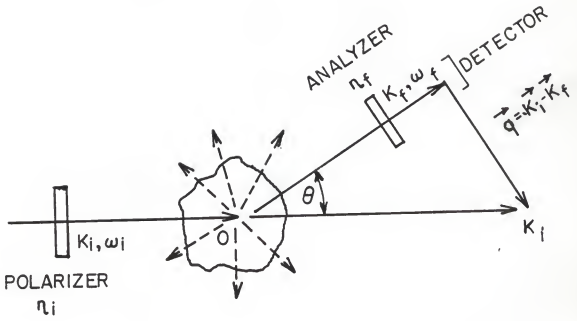
ANALYZER
n_f
K_f, ω_f
DETECTOR
$\vec{q}=\vec{K}_i-\vec{K}_f$
θ
K_i, ω_i
O
K_f
POLARIZER
n_i

The magnitudes of K_i and K_f are respectively $2\pi n/\lambda_i$ and $2\pi n/\lambda_f$, where λ_i and λ_f are the wavelengths in vacuum of the incident and scattered radiation and n is the refractive index of the scattering medium. It is usually the case of elastic scattering that the wavelength of the incident light is changed very little in the scattering process so that

$$|\vec{K}_i| \cong |\vec{K}_f|.$$

Thus,

$$q^2 = |\vec{K}_f - \vec{K}_i|^2 = K_f^2 + K_i^2 - 2\vec{K}_i \cdot \vec{K}_f = 2K_i^2 - 2K_i^2 \cos\theta = 4K_i^2 \sin^2 \theta/2$$

$$q = 2K_i \sin \theta/2 = \frac{4\pi n}{\lambda_i} \sin \theta/2.$$

2.2 Fluctuations and Time-Correlation Functions

In light-scattering experiments the incident light field is sufficiently weak that the system can be assumed to respond linearly to it. The basic problem is to describe the response of an equilibrium system to this weak incident field, or more precisely the changes of the light field (frequency shifts, polarization changes, etc.) due to its interaction with the system. This problem has been solved in general for weak probes. The major result of this theory, which is called 'linear response theory', is very simple. Whenever two systems are weakly coupled to one another (such as radiation weakly coupled to matter), it is only necessary to know how both systems behave in the absence of the coupling in order to describe the way in which one system responds to the other. Furthermore, the response of one system to the other is completely describable in terms of time correlation functions of dynamical variables.

Time-dependent correlation functions have been familiar for a long time in the theory of noise and stochastic processes. In recent years they have become very useful in many areas of statistical physics and spectroscopy. Correlation functions provide a concise method for expressing the degree to which two dynamical properties are correlated over a period of time.

Let us consider a property A that depends on the positions and momenta of all the particles in the system. By virtue of the thermal motions the particles are constantly jostling around so that their positions and momenta are changing in time, and so too is the property A. Although the constituent particles are moving according to Newton's equations (or Schrodinger's equation), their very number makes their motion appear to be somewhat random. The time dependence of the property A(t) will generally resemble a noise pattern given in Fig. 2.2.1.

As an example, let's consider the pressure on the wall of a cylinder containing a gas in equilibrium. The pressure on the wall at a given time is proportional to the total force on the wall, which in turn is a function of the distances of all the particles from the wall. As the particles move about, the total force fluctuates in time in a very finite manner. The pressure is therefore a fluctuating property. Suppose now that we could couple some kind of gauge to the wall that could respond rapidly to the pressure changes. The needle on this gauge would execute an erratic behavior - it would fluctuate. Since molecular motion is very rapid, the needle would jump around very rapidly. What would be reported as the pressure of the gas? The gauge should be read at a large number of time intervals and the results should be averaged. An average over a sufficiently long time (a time long compared with the period of the

Fig. 2.2.1. The property A(t) fluctuates in time as the molecules move around in the fluid. The time axis is divided into discrete intervals, Δt, and the time average $\langle A \rangle$ is assumed to be zero for convenience.

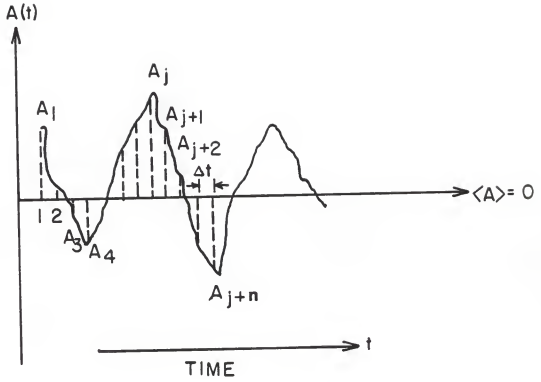
A(t)
A1
Aj
Aj+1
Aj+2
Δt
<A>= 0
1 2
A3
A4
Aj+n
t
TIME

fluctuation) would yield a fairly reliable pressure. If the same average were performed at a different time, essentially the same average value would be obtained. From this example we see that the measured bulk property of an equilibrium system is simply a time average

$$\bar{A}(t_o,T) = \frac{1}{T}\int_{t_o}^{t_o+T} A(t)\, dt \,. \tag{2.2.1}$$

Here t_o is the time at which the measurement is initiated and T is the time over which it is averaged. The average becomes meaningful only if T is large compared to the period of fluctuation. The ideal experiment would be one in which A is averaged over an infinite time,

$$\bar{A}(t_o) = \lim_{T\to\infty} \frac{1}{T}\int_{t_o}^{t_o+T} A(t)dt. \tag{2.2.2}$$

It can be shown that under certain general conditions this infinite time average is independent of t_o. In statistical mechanics it is usually assumed that this is valid. In Fig. 2.2.1 we see that the property A fluctuates about the time average which because of its independence of t_o can be expressed as

$$\langle A \rangle = \lim_{T\to\infty} \frac{1}{T}\int_{o}^{T} A(t)dt. \tag{2.2.3}$$

The noise signal A(t) in Fig. 2.2.1 displays the following features: The property A at the two times t, and $t + \tau$ can, in general, have different values so that $A(t + \tau) \neq A(t)$. Nevertheless, when τ is very small compared to time typifying the fluctuations in A, $A(t + \tau)$ will be very

close to A(t). As τ increases the deviation of $A(t + \tau)$ from A(t) is more likely to be non-zero. Thus, in some sense we can say that the value $A(t + \tau)$ is correlated with A(t) when τ is small but that this correlation is lost as τ becomes large compared with the period of the fluctuations. A measure of this correlation is the autocorrelation function of the property A which is defined by

$$\langle A(0)\ A(\tau)\rangle = \lim_{T\to\infty} \frac{1}{T} \int_0^T A(t)A(t + \tau)dt. \tag{2.2.4}$$

Let's Suppose that the time axis is divided into discrete intervals Δt, such that $t = j\Delta t$, $\tau = n\Delta t$, $T = N\Delta t$ and $t + \tau = (j+n)\Delta t$, and let's suppose further that the property A varies very little over the time interval Δt. From the definition of the integral it then follows that Eqs. (2.2.3) and (2.2.4) can be approximated by

$$\langle A\rangle \cong \lim_{N\to\infty} \frac{1}{N} \sum_{j=1}^{N} A_j \tag{2.2.5}$$

$$\langle A(0)A(\tau)\rangle \cong \lim_{N\to\infty} \frac{1}{N} \sum_{j=1}^{N} A_j A_{j+n} \tag{2.2.6}$$

where A_j is the value of the property at the beginning of the j^{th} interval. These sums become better approximations to the infinite time averages as $\Delta t \to 0$.

In optical mixing experiments, a correlator computes time-correlation functions of the scattered field in this discrete manner. Of course, in any experimental determination the averaging is done over a finite number of steps. It may be noted that many of the terms in the sum of Eq. (2.2.6) are negative. For example, in Fig. 2.2.1, $A_j A_{j+n}$ is negative. Consequently, this sum will involve some cancellation between

positive and negative terms. Now let's consider the case $\langle A(0)A(0)\rangle$. The sum contributing to this is $\sum_j A_j A_j = \sum A_j^2$ since $A_j^2 \geq 0$ all the terms in the sum are positive and we expect the total to be large. What this implies is that

$$\sum_{j=1}^{N} A_j^2 \geq \sum_{j=1}^{N} A_j A_{j+n} \tag{2.2.7}$$

thus,

$$\langle A(0)^2\rangle \geq \langle A(0)A(\tau)\rangle. \tag{2.2.8}$$

It would appear that the autocorrelation function either remains equal to its initial value for all times τ, in which case A is a constant of the motion (a conserved quantity) or decays from its initial value which is a maximum. That is, we expect the autocorrelation function of a nonconserved, nonperiodic property will decay from its initial value $\langle A^2\rangle$. For times τ large compared to the characteristic time for the fluctuation of A, $A(t)$ and $A(t+\tau)$ are expected to become totally uncorrelated. Thus,

$$\lim_{T\to\infty} \langle A(0)A(\tau)\rangle = \langle A(0)\rangle\langle A(\tau)\rangle = \langle A\rangle^2.$$

That is, the time-correlation function of a nonperiodic property decays from $\langle A^2\rangle$ to $\langle A\rangle^2$ in the course of time. This is shown in Fig. 2.2.2.

2.3 Photon Correlation Spectroscopy

In this section we will describe PCS. A useful example of the application of this technique is to consider a suspension of particles in a liquid. The photons are scattered quasi-elastically by the particles in a solution, which are in random motion, causing phase shifts in the

Fig. 2.2.2. The time correlation function $\langle A(0)A(\tau)\rangle$. Initially this function is $\langle A^2\rangle$. For times very long compared to the correlation time, τ_A, the correlation function decays to $\langle A\rangle^2$.

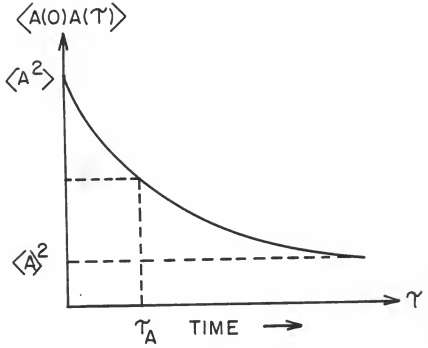
⟨A(0)A(τ)⟩
⟨A²⟩
⟨A⟩²
τ
τA
TIME

scattered light. This is similar to the frequency shift experienced with moving objects because of the Doppler effect. The spectrum of frequencies arising from the phase modulated scattered light is detectable only with a signal mixing or light beating technique. The high resolution measurement of these small frequency shifts is accomplished by translation of the spectrum originally at $\sim 10^{14}$ Hz to the audio frequency range, by either homodyne or heterodyne detection.

In heterodyne detection, the signal is beat or mixed with a strong 'local oscillator'. In the case of light scattering this local oscillator is the unshifted laser light which is mixed with the scattered light signal on the cathode of the photomultiplier tube. Homodyne detection uses a so-called self-beating process. The scattered light is mixed with itself on the cathode of the photomultiplier tube.

Previously particle size was determined using an analog power spectrum method. PCS, on the other hand, uses digital methods to determine the correlation function of the scattered light, the Fourier transform of the power spectrum. PCS counts the number of scattered photons per unit time interval and thus needs lower scattered light power than does the analog power spectrum method. Furthermore, PCS is more efficient with information measured at low light levels. Details about the homodyne and heterodyne detection technique and their respective correlation functions will be discussed later in this chapter.

2.4 Optical Mixing Technique

Optical mixing techniques are the optical analogs of the beating techniques developed in radio-frequency spectroscopy. They have made possible the application of light scattering in the study of the dynamics

of relatively slow processes such as macromolecular diffusion, the dynamics of fluctuations in the critical region, and the motility of microorganisms.

In optical mixing methods no wavelength filter is inserted between the scattering medium and the photomultiplier. The scattered light impinges directly on the PM cathode. Since the phototube is a square-law detector, its instantaneous current output is proportional to the square of the incident electric field $i(t) \propto |E(t)|^2$. The PM output is then passed to an autocorrelator, which calculates its time autocorrelation function

$$\langle i(t)i(0)\rangle = \beta \langle |E(0)|^2 \; |E(t)|^2 \rangle. \tag{2.4.1}$$

Here β is a proportionality constant. The correlator can be used in either a 'digital' or an 'analog' mode. In the digital mode one counts and then autocorrelates current photopulses due to photons, whereas in the analog mode, one directly autocorrelates the fluctuations in the PM output current.

For the purpose of discussing the differences between heterodyne and homodyne scattering, two scattered field autocorrelation functions are defined.

$$I_1(t) \equiv \langle E_s(0) \; E_s^*(t) \rangle \tag{2.4.2}$$

$$I_2(t) \equiv \langle |E_s(0)|^2 \; |E_s(t)|^2 \rangle. \tag{2.4.3}$$

Here E_s is the scattered field and the asterisk implies complex conjugation. We also introduce two more functions dependent only on the wave phases ψ,

$$F_1(\vec{q},t) = \langle \psi \; (\vec{q},0)\psi^*(\vec{q},t) \rangle \tag{2.4.4}$$

$$F_2(\vec{q},t) = \langle|\psi(\vec{q},0)|^2 \; |\psi^*(\vec{q},t)|^2\rangle. \tag{2.4.5}$$

We see that

$$I_1 \sim F_1 \text{ and } I_2 \sim F_2$$

where

$$\psi(\vec{q},t) \equiv \sum_{j=1}^{N}{}' \exp i\vec{q}\cdot\vec{r}_j(t). \tag{2.4.6}$$

The prime on the sum for ψ is used to indicate summation only over particles which are in the scattering volume V at time t. When a particle leaves V, it ceases to contribute to the scattering until it re-enters V. $\vec{r}_j(t)$ indicates the position of the j^{th} particle at time t relative to some reference. To eliminate the restricted sum in Eq. (2.4.6), we introduce the function P(r) which is called the amplitude function in the scattering volume so that

$$\psi = \sum_j e^{i\vec{q}\cdot\vec{r}_j} P(\vec{r}_j) \tag{2.4.7}$$

The summation indicated in the above equation is performed over all the scattering centers within the fluid. The fact that only a small portion of the centers are actually illuminated and detected is taken into account by the electric field amplitude weighting function P(r).

2.4.1 Heterodyne Correlation Function

In the heterodyne method, a small portion of the unscattered laser light is mixed with the scattered light on the photomultiplier cathode. If $E_{Lo}(t)$ represents the local oscialltor electric field, then the electric field at the PM is the superposition of $E_{Lo}(t)$ and $E_s(t)$ and thus the autocorrelation function of the PM output becomes

$$\langle i(0)i(t)\rangle = \beta \langle |E_{Lo}(t) + E_s(t)|^2 \; |E_{Lo}(0) + E_s(0)|^2 \rangle. \quad (2.4.1.1)$$

If $|E_{Lo}(t)| >> |E_s(t)|$, which can be obtained by proper choice of experimental conditions, and if we also assume a) fluctuations of the local oscillator field are negligible, and b) the local oscillator field and the scattered field are statistically independent, i.e. $\langle I_s I_{Lo} \rangle = \langle I_{Lo} \rangle \langle I_s \rangle$, equation (2.4.1.1) gives

$$\langle i(0)i(t)\rangle \cong \beta [I_{Lo}^2 + 2 I_{Lo} \mathrm{Re} I_1(t)] \quad (2.4.1.2)$$

where, $I_{Lo} = \langle |E_{Lo}|^2 \rangle$

and $\mathrm{Re}I_1(t)$ is the real part of $I_1(t)$. To proceed further, we need to calculate $F_1(t)$ which is proportional to $I_1(t)$. We calculate F_1 for a system of particles that are:

1) diffusing

2) flowing with velocity $\vec{V}$.

The relationship between the distance vectors is shown in Fig. 2.4.1.1. L is measured from some fixed point in the laboratory, in this case the surface of the photomultiplier tube, and is a constant vector ending at some fixed reference point within the fluid, here the center of the scattering volume. The vector $\vec{r}_n'(t)$ gives the position of the n^{th} particle in the fluid at time t relative to the fixed reference point.

It is considered that the fluid undergoes a translational motion with respect to the detector at velocity $\vec{V}$. In this case the transformation made is

$$\vec{r}_n'(t) = \vec{r}_n(t) + \vec{V}t. \quad (2.4.1.3)$$

$\vec{r}_n(t)$ is the position of the n^{th} scattering center measured relative to the moving fluid rather than with respect to the stationary

Fig. 2.4.1.1. The relationship between the distance and velocity vectors.

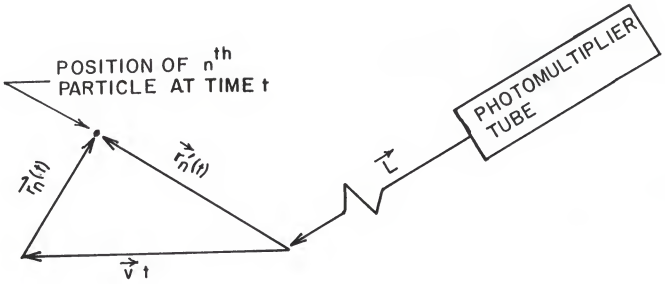
POSITION OF n^{th}
PARTICLE AT TIME t
$\vec{r}_n(t)$
$\vec{r}_n(t)$
$\vec{v}\,t$
$\vec{L}$
PHOTOMULTIPLIER
TUBE

(laboratory) frame of reference that was used for $\vec{r}_n'(t)$. The vector $\vec{r}_n(t)$ is still time dependent because the scattering center can undergo random, diffusive motions with respect to the fluid. The fluid velocity may also be a function of position. The transformation in Eq. (2.4.1.3) is done to separate $\vec{V}$ from Brownian motion.

We now substitute Eq. (2.4.1.3) into Eq. (2.4.7) which is then substituted into Eq. (2.4.4) to give

$$F_1(\vec{q},t) = \langle \sum_m e^{+i\vec{q}\cdot(\vec{r}_m(o))} P(\vec{r}_m(0)) \sum_n e^{-i\vec{q}\cdot(\vec{r}_n(t)+\vec{V}t)} P(\vec{r}_n(t)+\vec{V}t) \rangle$$

$$= \langle e^{-i\vec{q}\cdot\vec{V}t} \sum_{m,n} e^{i\vec{q}\cdot(\vec{r}_m-\vec{r}_n(t))} P(\vec{r}_m(0)) P(\vec{r}_n(t)+\vec{V}t) \rangle \quad (2.4.1.4)$$

where <---> represents two ensemble averages

1) One over the displacement, $\delta\vec{r}_{m,n}(t) \equiv \vec{r}_n(t) - \vec{r}_m(0)$ due to diffusion, and

2) One over the initial positions $\vec{r}_n(0)$.

We write both these ensemble averages explicitly as

$$F_1(\vec{q},t) = e^{-i\vec{q}\cdot\vec{V}t} \langle\langle \sum_{mn} e^{i\vec{q}\cdot\delta\vec{r}_{m,n}(t)} P(\vec{r}_m(0)) P(\vec{r}_n(t)+\vec{V}t) \rangle\rangle \quad (2.4.1.5)$$

Where the double bracket denotes that the ensemble average involves an average over initial positions of the scattering centers and an average over their displacement relative to the fluid.

Now, $\delta\vec{r}_n = \vec{r}_n(t) - \vec{r}_n(0)$

Since $\delta\vec{r}_n$, the distance moved by the n^{th} scattering center relative to the fluid, is assumed independent of the original particle position, $\vec{r}_n(0)$,

$$F_1 = e^{-i\vec{q}\cdot\vec{V}t} \sum_{mn} \langle e^{i\vec{q}\cdot\delta\vec{r}} \rangle_{\delta r} \langle P(\vec{r}_m(0)) P(\vec{r}_n(t) + \vec{V}t) \rangle_{r(0)}. \qquad (2.4.1.6)$$

The average of all the terms for m≠n is zero if the scattering centers are randomly placed throughout the fluid.

$$F_1 = e^{-i\vec{q}\cdot\vec{V}t} \sum_{m} \langle e^{i\vec{q}\cdot\delta\vec{r}_m} \rangle \langle P_m(0) P_m(t) \rangle = N\, e^{-i\vec{q}\cdot\vec{V}t} \langle e^{i\vec{q}\cdot\delta\vec{r}} \rangle \langle P(0)P(t) \rangle \qquad (2.4.1.7)$$

In many cases of practical interest, especially in light scattering experiments in which the fluid is static, the effect of the term $P(\vec{r})$ is small. In other words, if $\exp(i\vec{q}\cdot\vec{r})$ goes through many revolutions as it passes through the sample volume, then to a good approximation $P(\vec{r})$ can be replaced by unity. However, when the fluid is moving due to the bulk motion the effect of the finite illuminated volume can be very pronounced and, in fact, causes considerable broadening of the signal. For the situation of concern to us where we have flow, we need to evaluate the expression for $\langle P(r_m(0))\, P(r_n(t) + Vt) \rangle$ in Eq. (2.4.1.7).

It is now useful to introduce the Van-Hove 'self space-time correlation function' through the equation

$$F_s(\vec{q},t) = \langle e^{i\vec{q}\cdot\delta\vec{r}} \rangle = \int G_s(\vec{\delta r},t)\, e^{i\vec{q}\cdot\delta\vec{r}}\, d(\vec{\delta r}). \qquad (2.4.1.8)$$

In probability theory the Fourier transform of a probability distribution function is called the characteristic function of the distribution. Thus $F_s(\vec{q},t)$ is the characteristic function of $G_s(\delta r,t)$. $F_s(\vec{q},t)$ can be determined from light scattering. Thus, $G_s(\delta r,t)$ can be determined by an inverse Fourier transform

$$G_s(\delta r,t) = (2\pi)^{-3} \int F_s(\vec{q},t)\, e^{-i\vec{q}\cdot\delta r}\, d(\delta r) \qquad (2.4.1.9)$$

$G_s(\vec{\delta r},t)$ is the probability distribution for a particle to suffer a displacement δr in time t and is called Van Hove self space-time correlation function. Suppose that there is a solution such that at time t=0 a macromolecule is in the neighborhood of the origin. As time progresses it is expected that the macromolecule will execute small excursions - perform a random walk - so that after time t this particle will diffuse into the neighborhood of $\vec{\delta r}$ with probability $G_s(\vec{\delta r},t)d(\vec{\delta r})$. It is well known from the theory of random walk that the diffusion equation (for times long compared to the velocity correlation time) describes this probability. Then $G_s(\vec{\delta r},t)$ can, to a very good approximation, be regarded as the solution to the diffusion equation

$$\frac{\partial}{\partial t} G_s(\vec{\delta r},t) = D\nabla^2 G_s(\vec{\delta r},t) \qquad (2.4.1.10)$$

where D is the diffusion coefficient.

The spatial Fourier transform of Eq. (2.4.1.10) is

$$\frac{\delta}{\delta t} F_s(\vec{q},t) = -q^2 D F_s(\vec{q},t).$$

The solution of this equation subject to the boundary condition $F_s(\vec{q},0)=1$ is

$$F_s(\vec{q},t) = \langle e^{iq\cdot\delta r}\rangle = \exp(-q^2Dt). \qquad (2.4.1.11)$$

For simple diffusional case the heterodyne correlation function is

$$C(\vec{q},t) = \langle i(0)i(t)\rangle = \beta[I_{Lo}^2 + 2 I_{Lo}\langle N\rangle \exp(-Dq^2t)]$$

As stated earlier β is a proportionality constant, I_{Lo} is a constant proportional to the intensity of the local oscillator and $\langle N\rangle$ is the

average number of particles in the scattering volume. The time dependent part of this function is $C(\vec{q},t) \propto \langle N \rangle \exp(-\vec{q}^2 Dt)$

We now continue with the solution of Eq. (2.4.1.7). Consider a realistic P(r) for a laser which is

$$P(r) = e^{-r^2/4\sigma^2}. \qquad (2.4.1.12)$$

The above expression for P(r) is true for spherically symmetric sample volume. We know that the laser beam is cylindrically symmetric. But the use of the above expression was justified because of its simplicity and because the spherical symmetry approximation for the scattered beam is a reasonable approximation.

Then

$$\langle P\ P(t) \rangle = \int e^{-r^2/4\sigma^2}\ e^{-\frac{(\vec{r}+\vec{V}t)^2}{4\sigma^2}}\ d^3r.$$

Let $d^3r = dx \cdot dy \cdot dz$, also let $V = V_z$, i.e. the velocity is only in one direction. Then

$$\int_{-\infty}^{+\infty} e^{-r^2 4\sigma^2\ \frac{(\vec{r}+\vec{V}t)^2}{4\sigma^2}}\ dx\ dy\ dz = e \int_{-\infty}^{+\infty} -x^2/2\sigma^2 dx \int_{-\infty}^{+\infty} e^{-y^2/2\sigma^2} dy \int_{-\infty}^{+\infty} e^{-\frac{Z^2-(z+Vt)^2}{4\sigma^2}}\ dz$$

$$\propto \int_{-\infty}^{+\infty} \frac{-z^2 - (z+Vt)^2}{4\sigma^2}\ dz$$

let $u = z - \frac{1}{2}b$, then
$du = dz$

$$= \int e^{-a(u+\frac{1}{2}b)^2 - a(u-\frac{1}{2}b)^2}\ du$$

$$= \int e^{-a(2u^2+\frac{1}{2}b^2)}\ du = e^{-ab^2/2} \int e^{-2au^2}\ du \propto e^{-ab^2/2}$$

where

$$a = \frac{1}{4\sigma^2}\ ,\ b = -vt,\ e^{-ab^2/2} = e^{-\frac{v^2t^2}{8\sigma^2}} \qquad (2.4.1.13)$$

Therefore,

$$F_1(\vec{q},t) = \langle N\rangle e^{-i\vec{q}\cdot\vec{V}t}\ e^{-Dq^2t}\ e^{-v^2t^2/8\sigma^2} \qquad (2.4.1.14)$$

So we see that the correlation function is proportional to the product of two exponentials, one has linear dependency on t which is the case for diffusion and the other has quadratic dependency on t which is the case for flow. For the situation of interest to us we have both of these together an exponential with the sum of t and t^2 terms.

2.4.2 Homodyne Correlation Function

Since in the homodyne method only the scattered light impinges on the photocathode, E(t) is equal to the scattered field $E_s(t)$, so that $\langle i(0)i(t)\rangle$ is proportional to $I_2(t)$ - which is called the homodyne correlation function. The amplitude of $E_s(t)$, the scattered field, is proportional to the instantaneous dielectric constant fluctuation in the scattering volume and, of course, fluctuates in the same manner.

As was defined before in Eq. (2.4.5)

$$F_2(\vec{q},t) = \langle|\psi^*(\vec{q},0)|^2|\psi(\vec{q},t)|^2\rangle,$$

where ψ defined in Eq. (2.4.7) turns out to be,

$$\begin{aligned}\psi(\vec{q},t) &= \sum_{j=1}^{N} \exp(i\vec{q}\cdot\vec{r}(t))\ P(\vec{r}(t)),\\ &= \sum e^{i\vec{q}\cdot(\vec{r}(t)+\vec{V}t)}\ P(\vec{r}(t)+\vec{V}t)\\ &= \sum e^{i\vec{q}\cdot\vec{V}t}\ e^{i\vec{q}\cdot\vec{r}(t)}\ P(\vec{r}(t)+\vec{V}t)\ .\end{aligned} \qquad (2.4.2.1)$$

Now we consider four particle j, k, ℓ, m because at time t=0, we have to have two ψ's, one complex conjugate of the other and the same at time t. Here again as in the heterodyne case we have two ensemble averages

1) over the displacement, $\delta\vec{r}^{(t)}_{m,n} = \vec{r}_n(t) - \vec{r}_m(0)$ due to diffusion, and

2) one over the initial positions $\vec{r}_n(0)$.

$$F_2 = \langle\langle \sum_{jk\ell m} e^{i\vec{q}\cdot\vec{r}_j(0)} P(\vec{r}_j(0)) e^{-i\vec{q}\cdot\vec{r}_k(0)} P(\vec{r}_k(0)) e^{i\vec{q}\cdot\vec{V}t} e^{+i\vec{q}\cdot\vec{r}_\ell(t)}$$

$$P(\vec{r}_\ell(t) + \vec{V}t)\ e^{-i\vec{q}\cdot\vec{V}t}\ e^{-i\vec{q}\cdot\vec{r}_m(t)} P(\vec{r}_m(t) + \vec{V}t)\rangle_{r(0)}\rangle_{\delta r} \qquad (2.4.2.2)$$

These terms simplify considerably for dilute solutions when the positions of different molecules are statistically independent. Then the term

$$\langle P(\vec{r}_j(0))P(\vec{r}_k(0))P(\vec{r}_\ell(t)+\vec{V}t)P(r_m(t)+Vt)\ \exp\ i\vec{q}\cdot[\vec{r}_\ell(t) - \vec{r}_j(0)]$$
$$\exp - i\vec{q}\cdot[\vec{r}_m(t) - \vec{r}_k(0)]\rangle$$

will be zero if any pair of the four particle indices are not equal. Suppose that the particle ℓ is distinct, the term factors due to the assumed particle independence into

$$\langle e^{i\vec{q}\cdot\vec{V}t}\ e^{i\vec{q}\cdot\vec{r}_\ell(t)} P(\vec{r}_\ell(t)+\vec{V}t)\rangle\langle P(\vec{r}_j(0))P(\vec{r}_k(0))P(\vec{r}_m(t)+\vec{V}t)\ \exp(i\vec{q}\cdot\vec{r}_j(0))$$
$$\exp(-i\vec{q}\cdot\vec{r}_k(0))\ \exp - (i\vec{q}\cdot\vec{V}t + i\vec{q}\cdot\vec{r}_m(t))\rangle$$

The first factor is simply the ensemble average of the quantity $\exp(i\vec{q}\cdot\vec{r}(t))$. If the system is homogeneous, the particles are distributed randomly so that the probability of finding particle ℓ in the neighborhood d^3r is $d^3r\ V_{Scat}^{-1}$. Where V_{Scat} is the illuminated volume of the sample. Thus,

$$\langle \exp(i\vec{q}\cdot\vec{r}_{\ell}(t)) \rangle = V_{Scat}^{-1} \int_{V_{Scat}} d^3r \; e^{i\vec{q}\cdot\vec{r}} \to \delta(q).$$

For scattering in other than the forward direction ($q \neq 0$), this quantity is zero. Consequently only two kinds of terms survive, those for which a) j=k, ℓ=m including k=j=ℓ=m and b) j=m, k=ℓ, j≠k.

For case a)

$$F_2 \equiv F_2' = \langle\langle \sum_{j,\ell} P^2(\vec{r}_j(0)) \; P^2(\vec{r}_{\ell}(t) + \vec{V}t) \rangle\rangle. \qquad (2.4.2.3)$$

For case b)

$$F_2 \equiv F_2'' = \langle\langle \sum_{j \neq \ell} P(\vec{r}_j(0)) P(\vec{r}_k(0)) P(\vec{r}_k(t)+\vec{V}t) P(\vec{r}_j(t)+\vec{V}t) \; e^{-i\vec{q}\cdot\delta\vec{r}_j} \; e^{i\vec{q}\cdot\delta\vec{r}_k} \rangle\rangle. \qquad (2.4.2.4)$$

Now we consider these terms separately with the assumptions

1) $\delta r \ll Vt$, i.e. diffusion is much smaller than the bulk motion.

2) Spherical scattering volume for which $P(r) \sim e^{-r^2/4\sigma^2}$.

For case a, there is no dependence on δr. So $\langle A \rangle_{\delta r} = A$. Thus we need to perform an average over $\vec{r}(0)$. The average over initial positions can be performed by recognizing that the probability per unit volume of finding a scattering center is just ρ/N. Where ρ is N/V_{Scat}.

For case (a)

$$F_2' = \sum_{j \neq \ell} \frac{\rho^2}{N^2} \int e^{-r_j^2/2\sigma^2} \; e^{-(r_1+Vt)^2/2\sigma^2} \; d^3r_j d^3r_1$$

$$= \sum_{j \neq \ell} \rho^2/N^2 \; (\pi 2\sigma^2)^{3/2} \; (\pi 2\sigma^2)^{3/2} \qquad (2.4.2.5)$$

There are $N^2 - N$ terms of $\sum_{j \neq \ell}$ so

$$F_2' = \frac{N^2-N}{N^2}\,\rho^2\,(2\pi\sigma^2)^3 = \frac{N-1}{N}\,\rho^2(2\,\pi\sigma^2)^3 \qquad (2.4.2.6)$$

$(8\pi^3\sigma^6)$ can be regarded as the effective scattering volume squared (V_{Scat}^2) which gives $\frac{N^2-N}{N^2}\,\rho^2\,V_{Scat}^2 = N^2-N$.

Now considering $j=\ell=m=k$

$$F_2' = \sum_{j=\ell} \rho/N \int e^{-r_j^2/2\sigma^2}\; e^{-\frac{(r_j+Vt)^2}{2\sigma^2}}\; d^3r_j\; d^3\rho_j$$

$$= N\,\rho/N\; e^{-V^2t^2/4\sigma^2}\; V_{Scat}$$

$$= \rho\; e^{-V^2t^2/4\sigma^2}\; V_{scat} = N\; e^{-V^2t^2/4\sigma^2} \qquad (2.4.2.7)$$

or, $F_2' = N(N-1) + N\; e^{-V^2t^2/4\sigma^2}$ (2.4.2.8)

For Case (b)

we use $\delta r \ll Vt$, then the ensemble average separates

$$F_2'' = \sum_{j\neq\ell} \langle P(\vec{r}_j(0)P(\vec{r}_j(0)+\vec{V}t)P(\vec{r}_k(0))P(\vec{r}_k(0)+\vec{V}t)\rangle_{r(0)}$$
$$\langle e^{-i\vec{q}\cdot\delta\vec{r}_j}\; e^{i\vec{q}\cdot\delta\vec{r}_\ell}\rangle_{\delta r}$$

$$= \sum_{j\neq\ell} \langle PP(t)\rangle^2 |\langle e^{i\vec{q}\cdot\delta\vec{r}}\rangle|^2. \qquad (2.4.2.9)$$

It was shown before in Sec. 2.4.1 that

$$\langle PP(t)\rangle = e^{-V^2t^2/8\sigma^2}$$

$$\langle e^{i\vec{q}\cdot\delta\vec{r}}\rangle = e^{-Dq^2t}$$

which gives, $F_2'' = N(N-1)\; e^{-\frac{V^2t^2}{4\sigma^2}}\, e^{-2Dq^2t}$. (2.4.2.10)

Now F_2' and F_2'' are combined together to get F_2

$$F_2(q,t) = N(N-1)\ [1 + e^{-V^2t^2/4\sigma^2}\ e^{-2Dq^2t}] + N\ e^{-\frac{V^2t^2}{4\sigma^2}}. \qquad (2.4.2.11)$$

for a Poisson distribution

$\langle N(N-1)\rangle = \langle N^2\rangle - \langle N\rangle = \langle N\rangle^2$, which gives

$$F_2(\vec{q},t) = \langle N\rangle^2\ [1 + e^{-V^2t^2/4\sigma^2}\ e^{-2Dq^2t}] + \langle N\rangle\ e^{-V^2t^2/4\sigma^2}. \qquad (2.4.2.12)$$

Again we see that the correlation function is proportional to the product of two terms for the situation of interest to us. One of these terms is exponential which arises due to Brownian diffusion and the other is a Gaussian, arising due to the bulk motion.

3.0 EXPERIMENTAL APPROACH

The experimental chapter consists of four different sections, the apparatus, the analysis routine, the initial experiment, and the final experiment resulting in the conclusion.

3.1 Optical Component Arrangement

The optical system is illustrated in Fig. 3.1.1, where the principal components are shown in their usual relative positions. An aluminum slab, 132 cm by 100 cm by 6 cm, formed the main body of the optical table. Onto this slab was rigidly mounted a 6 mm thick sheet of mild steel so that magnetic optical holders could be used. This composite table top was supported by four sand filled concrete legs. An optically straight entruded magnesium rail was mounted to the table top. One part of this rail was fixed rigidly to the table, but the other part pivoted about a pin located below the center point of the scattering volume. Onto this rail the light collection assembly was mounted. A model 165-07 Spectra-physics Argon Ion Laser with a model 265 power supply was used for the majority of the measurements. The laser was located on a separate table near the main optical table. The laser beam was steered by two front surface mirrors, and then focused into the sample by a lens. As the laser was operated in the TEM_{oo} mode, the beam profile was Gaussian. The scattering volume was the intersection of the cylinders formed by the focused laser beam and the cylinder formed by the field of view of the collection optics.

The photomultiplier tube (PMT) used in the experiment monitored the light scattered about a certain angle. The PMT, an ITT FW 130, was mounted on the pivoted optical rail. The housing for this tube is shown

Fig. 3.1.1. Optical system showing the major components in their relative locations.

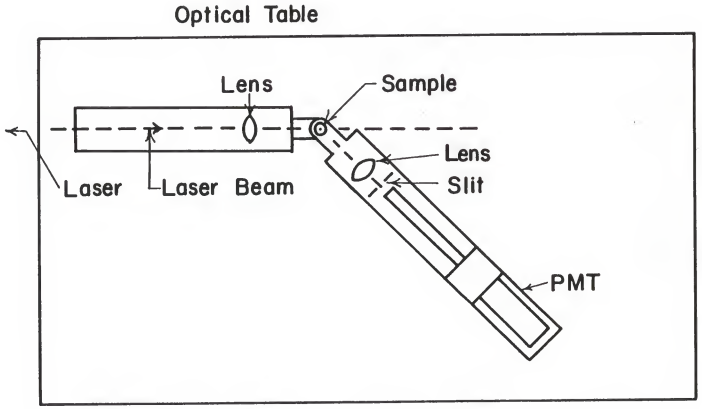
Optical Table
Lens
Sample
Lens
Slit
Laser
Laser Beam
PMT

in Fig. 3.1.2. The output from the FW 130 was fed through a Products for Research Inc. model 1102 modular amplifier-discriminator, which converts the photo-pulses into TTL pulses. Thus converted, these pulses were sent to a Langley-Ford instruments, model 1096, digital correlator. The processing of the scattered light signal is shown in Fig. 3.1.3.

3.2 Data Analysis

A typical intensity autocorrelation function measured in an experiment in which laser light is scattered from a suspension of particles is shown in Fig. 3.2.1.

The measured intensity autocorrelation function can be expressed as

$$G^{(2)}(\vec{q},t) = a + b\,|g^{(1)}(\vec{q},t)|^2,$$

where $g^{(1)}(\vec{q},t)$ is the normalized electric field autocorrelation function, and $\vec{q}$ is the scattering wave vector, defined in Section 2.1.

For the simplest case of monodisperse particles, the field correlation is a single decaying exponential, $|g^{(1)}(\vec{q},t)| = \exp(-\Gamma t)$, where $\Gamma = Dq^2$ and D is the diffusion coefficient.

If the suspension contains a distribution of particle sizes or shapes, then $|g^{(1)}(\vec{q},t)| = \int_0^\infty F_K(\Gamma)\, e^{-\Gamma t}\, d\Gamma$ where $F_K(\Gamma)d\Gamma$ is the fraction of the total scattered intensity contributed by particles with decay rates in the range Γ to $\Gamma + d\Gamma$. $\int_0^\infty F_K(\Gamma)d\Gamma = 1$. The n^{th} moment of the decay rate distribution is given by

$$\mu_n = \int_0^\infty F_K(\Gamma)(\Gamma - \langle\Gamma\rangle)^n\, d\Gamma$$

where $\langle\Gamma\rangle$ is the average decay rate, $\langle\Gamma\rangle = \int_0^\infty \Gamma F_K(\Gamma)d\Gamma$. If the polydispersity is not too great, the field autocorrelation function is only

Fig. 3.1.2. The housing for the ITTFW130 Photomultiplier tube and amplifier-discriminator.

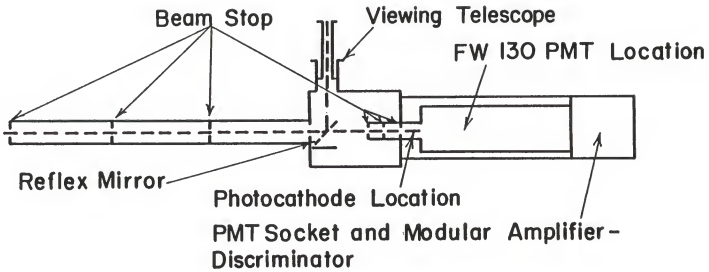
Beam Stop
Viewing Telescope
FW 130 PMT Location
Reflex Mirror
Photocathode Location
PMT Socket and Modular Amplifier-
Discriminator

Fig. 3.1.3. Data acquisition system for scattering measurement.

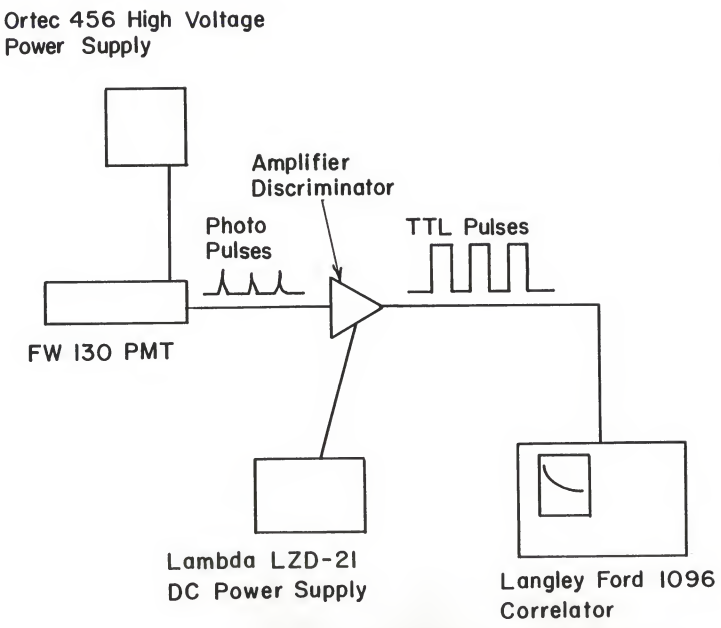
Ortec 456 High Voltage
Power Supply
Amplifier
Discriminator
Photo
Pulses
TTL Pulses
FW 130 PMT
Lambda LZD-21
DC Power Supply
Langley Ford 1096
Correlator

Fig. 3.2.1. A typical intensity auto-correlation function.

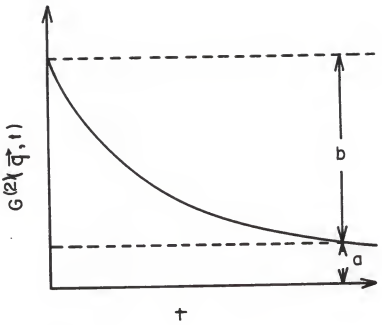
$G^{(2)}(\vec{q}, t)$
b
a
t

slightly non-exponential and we can write its natural logarithm in the form

$$\ln |g^{(1)}(\vec{q},t)| = -\langle\Gamma\rangle t + \frac{1}{2!}\mu_2 t^2 - \frac{1}{3!}\mu_3 t^3 + \ldots .$$

The coefficients of the terms in t, t^2, t^3, etc. are called the first, second, third cumulants, respectively.

Two parameters that are frequently used to characterize particle distributions are (1) the average decay rate $\langle\Gamma\rangle$ which in the case of small particles, is related to the diffusion coefficient by

$$D = \langle\Gamma\rangle/q^2, \qquad (3.2.1)$$

and (2) the polydispersity parameter $\mu_2/\langle\Gamma\rangle^2$ which is the ratio of the variance (the square of the standard deviation) to the square of the average of the decay rate distribution. The polydispersity parameter is a measure of the width of the distribution, but does not provide any information about its shape (i.e., whether the distribution is uni- or bimodal, skewed, etc.). The higher order moments are increasingly difficult to measure experimentally and are accessible only when the data are of very high precision. The analysis program in the Langley-Ford correlator calculates the two parameters $\langle\Gamma\rangle$ and $\mu_2/\langle\Gamma\rangle^2$ by performing a weighted, least-squares fit of a quadratic equation to the natural log of the measured correlation function $G^{(2)}(\vec{q},t)$ after the baseline has been subtracted. There are two possible choices for the baseline: the average of the last 8 channels of the measured correlation function or the theoretical baseline. Either may be selected from the keyboard.

When the analysis is complete, the results appear on the display screen of the correlator. The b/a ratio, $\langle\Gamma\rangle$ and $\mu_2/\langle\Gamma\rangle^2$ are calculated

and the values given. The diffusion coefficient may be calculated from Eq. (3.2.1). If the particles are assumed to be spherical, average diameter d may be calculated from the well known Stokes-Einstein equation

$$D = \frac{KT}{3\pi\eta d} .$$

Here K is Boltzmann's constant, T is the absolute temperature and η is the solvent viscosity.

From Eq. (2.4.2.12), we see for a system of particles that are both diffusing and flowing past the scattering volume with velocity v, that when the average number of particles <N> in the scattering volume is large, the time dependent part of the homodyne correlation function is related to t as shown below

$$C \propto \langle N \rangle^2 \left(\exp(-2q^2 Dt - \frac{v^2 t^2}{4\sigma^2}) \right)$$

or

$$C \propto e^{-t/\tau_1 - \frac{t^2}{\tau_2^2}} .$$

Where $\tau_1 = \frac{1}{2\Gamma}$ and $\tau_2 = \frac{2\sigma}{v}$ and $\Gamma = Dq^2$. τ_1 is the correlation time due to diffusion and τ_2 is the beam transit term due to bulk motion. In practical cases we have a background noise with the spectrum for which

$$C = A_1 e^{-t/\tau_1 - t^2/\tau_2^2} + B$$

from which it follows that

$$-\frac{1}{t} \ln \frac{C-B}{A_1} = \frac{1}{\tau_1} + \frac{t}{\tau_2^2} .$$

If we denote the L.H.S. of the above equation by Y,

$$Y = \frac{1}{\tau_1} + \frac{t}{\tau_2^2} .$$

A plot of Y against t should give us a straight line with the Y intercept of $1/\tau_1$ and a slope of $1/\tau_2^2$. Such a slope-intercept (SI) graph should make the analysis easier. τ_2 is inversely proportional to V. If we make a plot of the slope of the slope-intercept plot against flow rate squared, we should get a straight line from which we should be able to find the beam width σ. We shall call this the S plot. On the other hand, if we have a distribution of particle sizes in the scattering volume, as shown previously in this Section, for homodyne detection we will have for pure diffusion

$$C = A_1 \exp(-2\langle\Gamma\rangle t + \mu_2 t^2) + B$$

So as before,

$$Y = \frac{1}{\tau_1} - \mu_2 t.$$

We now see that if we have polydispersity then for pure diffusional system a plot of Y against t will give us a straight line with negative slope rather than a line parallel to the t axis expected for the monodisperse case. The intercept in Y axis will be the same, $1/\tau_1$. The negative slope of the line with polydispersity will be μ_2, the second cumulant.

When we have polydispersity and we are flowing at a lower rate then the relative magnitude of μ_2 and $1/\tau_2$ will determine the direction and magnitude of the slope.

Afterpulsing is the presence of spurious pulses after true pulses within the photomultiplier tube and may be regarded as a defect of the tube itself. The SI plot for sample time $\leq 10^{-5}$ sec gave us an indication that we might be getting into the problem of photomultiplier afterpulsing. For sample times of the order of 10^{-6} sec it became obvious. Since afterpulsing only effects the first few channels of the spectrum we felt that it would be worthwhile to modify our analysis to ignore these first few channels. Thus,

$$C(t) = A \exp - (t/\tau_1 + t^2/\tau_2^2)$$

$$C(n\Delta t) = A \exp - (n\Delta t/\tau_1 + n^2\Delta t^2/\tau_2^2)$$

where n is the channel number and Δt is the sample time.

$$Y(n) = -\frac{1}{n} \ln \frac{C(n\Delta t)}{C(0)} = \frac{\Delta t}{\tau_1} + \frac{n\Delta t^2}{\tau_2^2}$$

where $C(0) = A$

Now redoing at $C(1)$

$$Y^1(n) = -\frac{1}{n-1} \ln \frac{C(n)}{C(1)} = \frac{\Delta t}{\tau_1} + (n+1)\frac{\Delta t^2}{\tau_2^2}$$

$$Y(0) = \frac{\Delta t}{\tau_1}, \quad Y^1(0) = \frac{\Delta t}{\tau_1} + \frac{\Delta t^2}{\tau_2^2}, \quad Y^1(-1) = \frac{\Delta t}{\tau_1}$$

So $Y(0) = Y^1(-1)$, which gives $Y(n) = Y^1(n-1)$

Similarly

$$Y^m(n) = -\frac{1}{n-m} \ln \frac{C(n)}{C(m)} = \frac{\Delta t}{\tau_1} + (n+m)\frac{\Delta t^2}{\tau_2^2}$$

Thus $Y^m(n-m) = Y(n)$.

The mathematics above show that we may shift the Y-plot over by m. Changing m, shouldn't give any change in the slope and intercept of the SI plot if the axis is shifted properly. This allows us to ignore the first few channels which may be affected by the afterpulsing yet still are able to pull-out the correct τ_1 and τ_2.

3.3 Initial Experiment

The main idea behind this thesis was to understand light scattering from flowing Brownian motion particles applying PCS, and to be able to separate the correlation time due to diffusion from the beam transit term, which arises from the bulk motion of the fluid in which the particles are suspended. With this idea in mind, the first system studied was a non-flowing aqueous suspension of polystyrene latex microspheres. Systems composed of monodisperse polystyrene latex microspheres in aqueous suspension represent an established standard against which to verify the operation of the PCS system. Three sizes of Dow Chemical microspheres with nominal diameters 0.091μ ± 0.0058μ, 0.261μ ± .0031μ, and 0.330μ ± .0040μ, were suspended in dilute (10^{-5} volume %) solution. The measurements were conducted at four different scattering angles, 90°, 60°, 45°, and 30°. The sizes inferred from the diffusion constant measured with PCS agreed to within 3% of the manufacturer's stated sizes.

As shown previously, the scattering vector q equals $\frac{4\pi n}{\lambda_1} \sin \theta/2$. For a purely diffusional process, the correlation functions for heterodyne and homodyne cases are proportional to e^{-Dq^2t} and e^{-2Dq^2t}, respectively. Accordingly, τ_1 becomes equal to $(Dq^2)^{-1}$ and $(2dq^2)^{-1}$ for heterodyne and homodyne cases, respectively. Thus the logarithm of the

inverse correlation time of such a system will vary linearly with the logarithm of the sine of half the scattering angle, $\theta/2$. Furthermore, such a plot should have a slope of 2. This test was also performed. Figure 3.3.1 indicates that the dynamic light scattering from the polystyrene system yield a slope close to 2.

Next we tried to set up our flow system so that the scattering particles had translational motion with respect to the scattering volume. The system is shown in Fig. 3.3.2. It consists mainly of a 5 gallon overhead tank which contained the stock solution. The solution concentration used was the same as was used to study our non-flow system. A 3 ft. long glass tube 1 cm in diameter was connected to the bottom of this tank with tygon tubing. The laser beam was directed into this glass tube. The glass tube was held vertically and arrangements were made to keep it straight and free from vibration. The lower end of the tube was connected through tygon tubing to the flow meter. Another piece of tygon tubing connected the flow meter to a flow control valve. At the other end of the control valve a piece of tygon tubing was attached, the other end of which was connected to the lower level tank which has a capacity of about a gallon. From the lower level tank through a variable speed pump the solution can be taken to the overhead tank. There is also an overflow line from the overhead to the lower level tank.

Most of the measurements for the flow system were made at 90°. We filtered the distilled water before making the solutions. The overhead tank was then filled with this filtered water. The polystyrene particles were added in some filtered water in the lower level tank. Then the solution was mixed well by circulating the solution through the system for considerable length of time.

Fig. 3.3.1. A graph showing inverse correlation time versus Sin $\theta/2$ for a non-flowing system of Brownian particles of $d = 0.091\mu$. The line has a slope of 2.03.

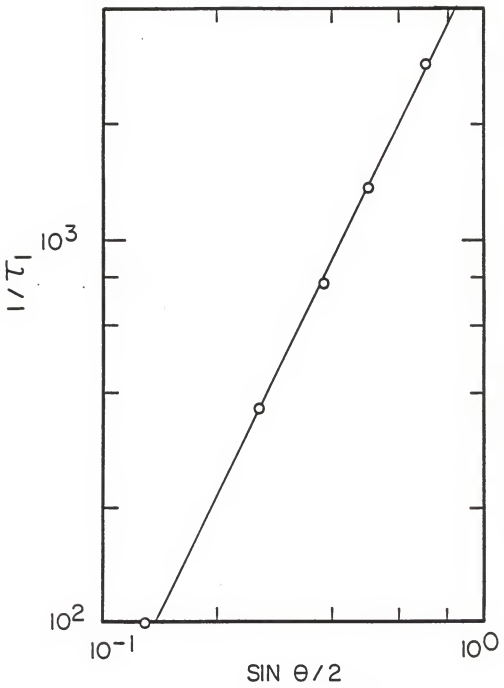
$1/\tau_1$
10^3
10^2
10^{-1}
10^0
SIN $\theta/2$

Fig. 3.3.2. The initial experimental set-up.

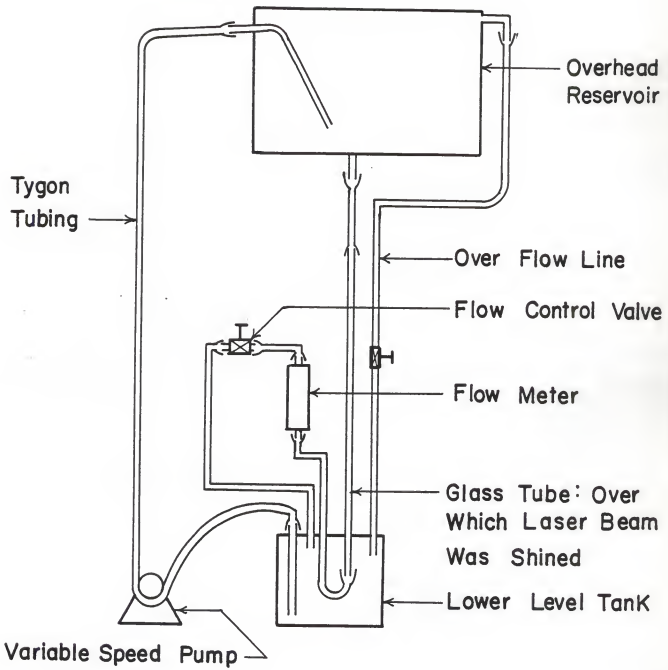
Overhead
Reservoir
Tygon
Tubing
Over Flow Line
Flow Control Valve
Flow Meter
Glass Tube: Over
Which Laser Beam
Was Shined
Lower Level TanK
Variable Speed Pump

We took some data for our flow system at flows of about 0.1 gallon per minute (GPM) and 0.2 GPM. In the way we analyzed our data as discussed previously, the slope of the line was measured. This value of the slope was not found to agree with the calculated value of the slope. So we thought that polydispersity in the solution might have resulted in this discrepancy. So we next tried to see if this was the case.

To observe the effect of polydispersity we took some data with the same solution but for the non-flowing case. A typical plot of the data is shown in Fig. 3.3.3. The plot shows a negative slope. The slope and intercept of the line agree well with the values found from the curve fitting routine of the correlator. Thus, it was found that polydispersity caused by a distribution of particle sizes was causing some problem in analyzing our data for the flow system.

We then thought of cleaning up our whole flow system and of making new solutions with newly filtered water, so as to eliminate the polydispersity in the solution as much as possible. In this way a new solution was made with a concentration of about 6.7×10^{8} cm^{-3} of polystyrene particles of 0.261 μ diameter. We took data for the non-flow system and made the plot. The SI plot of the data is shown in Fig. 3.3.4. As we see from the plot we were not getting a straight line as we were expecting. From the correlator fitting routine we did get Γ and μ_2, the first and second cumulant, respectively. If, however, Γ obtained from the correlator fit program was used to indicate the proper Y-intercept, then a line passing through this point and data at large time had a slope that gave the second cummulant reasonably close to the value found from the correlator fit. The data points at smaller t were

Fig. 3.3.3. A typical SI plot of a nonflowing system showing polydispersity with negative slope. Fit is to the function $c = e^{-2\Gamma t + \mu_2 t^2}$. Particles are of nominal diameter 0.091 μ. Taking $\Gamma = 2.4 \times 10^3$ sec^{-1} and μ_2 as slope of the line, μ_2/Γ^2 compares well with the fit program value.

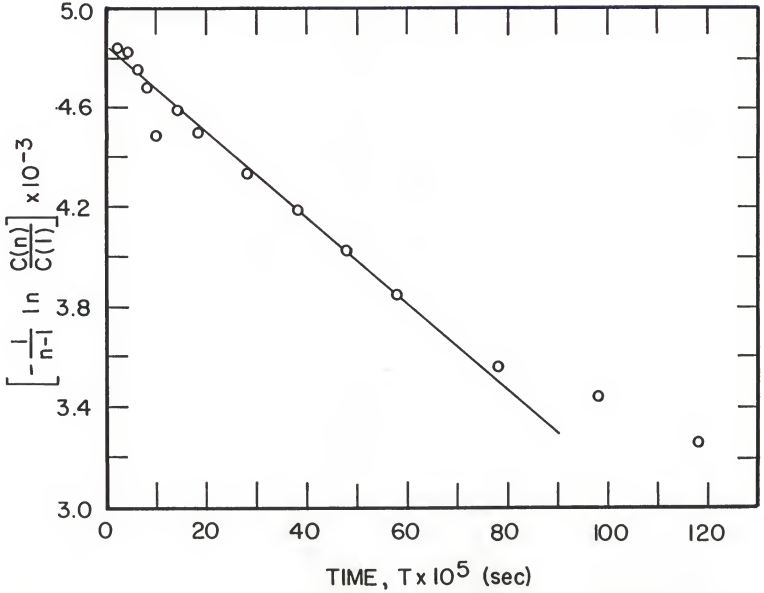
5.0
4.6
4.2
3.8
3.4
3.0
0
20
40
60
80
100
120
$\left[-\frac{1}{n-1} \ln \frac{C(n)}{C(1)}\right] \times 10^{-3}$
TIME, T x 10^5 (sec)

Fig. 3.3.4. A typical SI plot showing multiple scattering, for particles of nominal diameter 0.261 μ with particle concentration of 6.7×10^8 cm^{-3}.

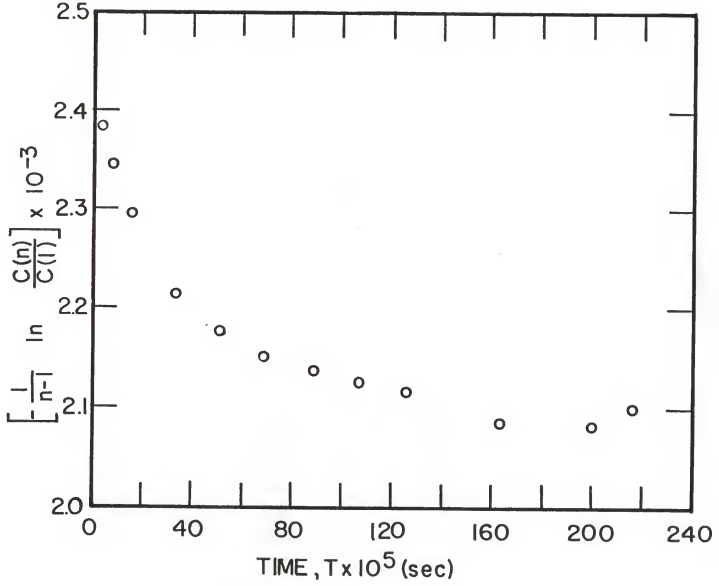
2.5
2.4
2.3
2.2
2.1
2.0
0
40
80
120
160
200
240
$\left[-\frac{1}{n-1}\right] \ln \frac{C(n)}{C(1)} \times 10^{-3}$
TIME, $T \times 10^5$ (sec)

found to be off the line and they were much too high. We thought that these higher initial points which correspond to higher value of Γ may have resulted from multiple scattering from Brownian motion. Previous experiments by researchers show that the linewidth (inverse correlation time) increases monotonically with concentration. So as the extent of multiple scattering is a function of particle concentration, we wanted to see a concentration dependence for the linewidth. Starting with the original solution we had been taking data with, we made solutions of several different concentrations and took data for each of those solutions separately. What we found is that the initial points started coming down more and more as the solution was diluted more and more. When the original solution was diluted ten times, all the data points lined up to give us a straight line with the value of the Y-intercept matching reasonably well with the Γ value. So it was thought that the multiple scattering due to high particle concentration was causing the high value of Y-intercept. We decided to work with the concentration for which a reasonably good straight line was obtained.

We made a new solution of 0.261 μ diameter Particles and made a run for the non-flowing system. We started with a very small flow of 50 ml/min. Then we started increasing the flow in small increments to a maximum flow of 850 ml/min. The Reynolds numbers calculated at flowrates of 50 ml/min, 100 ml/min, 150 ml/min, 300 ml/min, 600 ml/min, and 850 ml/min are about 106, 212, 318, 637, 1279 and 1800 respectively. The Y-intercept of each of the plots should be the same, because the Y-intercept determines Γ, the first cumulant, which is proportional to the diffusion constant. From the plots it is evident that the

Y-intercepts are not yielding the same values for different flow rates. We plotted the Y-intercept against the flow rate as shown in Fig. 3.3.5 and found that the plot comes out to be a straight line increasing with flow. We suspect that if there is any type of turbulence present in the system, it will increase the diffusion of the particle in addition to that due to the Brownian motion. The existence of laminar or turbulent flow doesn't depend only on the Reynolds number. The Reynolds stresses which initiate turbulence may be present even with very small flows for which we expect the flow to be laminar. These stresses may be due to the various non-idealities in the system, like the roughness of the tube surface through which the fluid is flowing, the flow tube is disturbed by some means, or if the mean velocity fluctuation is not zero. Another point of consideration is the length of the section of the flow tube over which the velocity profile develops. The approximate length of straight pipe needed for completion of the final laminar flow velocity distribution

$$\frac{X_t}{D} = .05\ N_{Re}$$

where

X_t is the length of the pipe,

D is the diameter of the pipe, and

N_{Re} is the Reynolds number at which the flow exists.

For the highest Reynold's number we worked with for the 10 mm I.D. tube, this formula suggests that the velocity profile had just developed. The entrance disturbance may not, however, damp out right there.

We next tried to do the same set of experiments as we did for the 3 ft long 10 mm I.D. tube with a 4 ft long 6 mm. I.D. tube. The

Fig. 3.3.5. A graph of the Y-intercept of the SI plot versus flow rate for tube of 10 mm I.D. using the initial set-up.

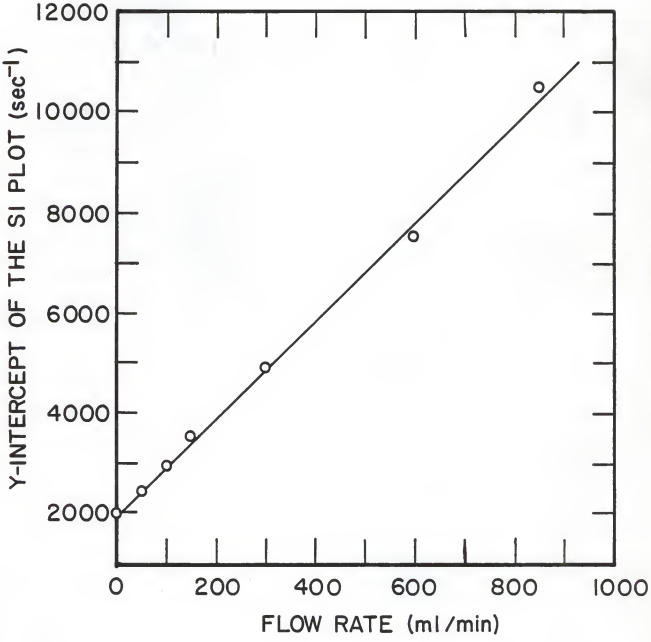
12000
10000
8000
6000
4000
2000
Y-INTERCEPT OF THE SI PLOT (sec⁻¹)
0
200
400
600
800
1000
FLOW RATE (ml/min)

connection to the 6 mm tube was still from a 10 mm tygon tubing. Thus the entrance disturbance is different for this smaller tube and is expected to be larger with this tube than with the 10 mm tube. Also with this tube there was a better chance for the velocity profile to develop fully, as indicated by the equation above, at the point where the laser beam was shown. The data was taken at flows of 50 ml/min, 100 ml/min, 350 ml/min, 450 ml/min, 600 ml/min, and 850 ml/min. The Reynolds number corresponding to these flows are, respectively, 177, 354, 1060, 1600, 2123 and 3007. The Y-intercept was plotted against flow rate as before. The plot is shown in Fig. 3.3.6. As with the 10-mm tube, the Y-intercept for the 6 mm tube was also found to increase with the flow rate, but the slope of the line for 6 mm tube was about 4.25 times larger than that of the 10 mm tube.

3.4 Final Experiment

To remove some of the uncertainties and disturbances in the flow system which we though may have effected our results, we decided to rebuild our flow system. We wanted to remove the pump, make the tube longer, minimize vibration of the tube, and also to have a smooth surfaced tube. The set-up we designed is shown in Fig. 3.3.7. In this system we made solutions in a separate jar and filled the upper level flask with the solution. We filled the rest of the sections of the system with the solution with the help of the pump. Once that was done, the pump is no longer needed. Using the flow and control valve right after the flow-meter, we adjusted the flow, and once the upper level tank is about to empty, we stopped the flow, poured the solution in the lower level tank into the one at the top, and then restarted the flow.

Fig. 3.3.6. A graph of the Y-intercept of the SI plot versus flow rate for tube of 6 mm I.D. using the initial setup.

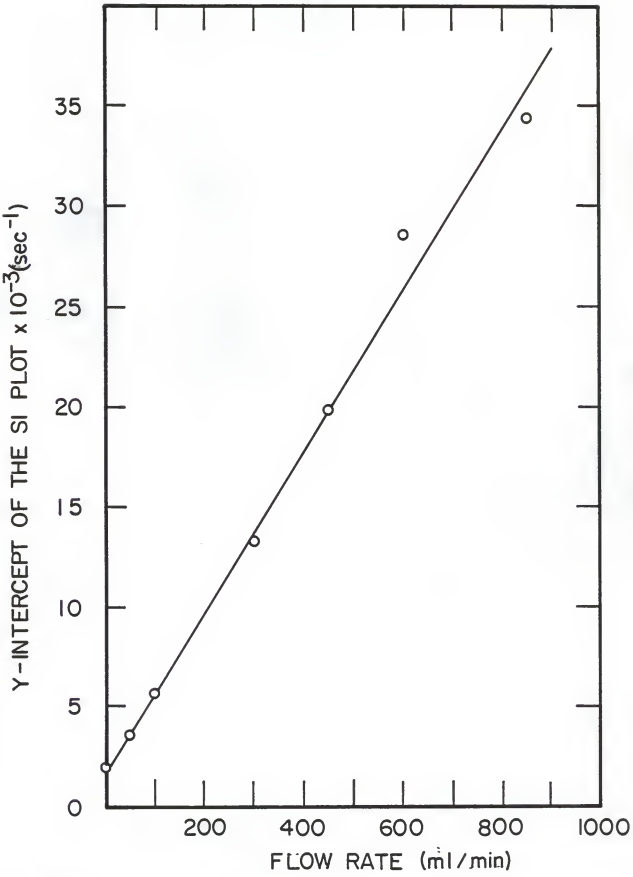
Y-INTERCEPT OF THE SI PLOT x 10^{-3}(sec^{-1})
0
5
10
15
20
25
30
35
200
400
600
800
1000
FLOW RATE (ml/min)

Fig. 3.3.7. The revised flow system.

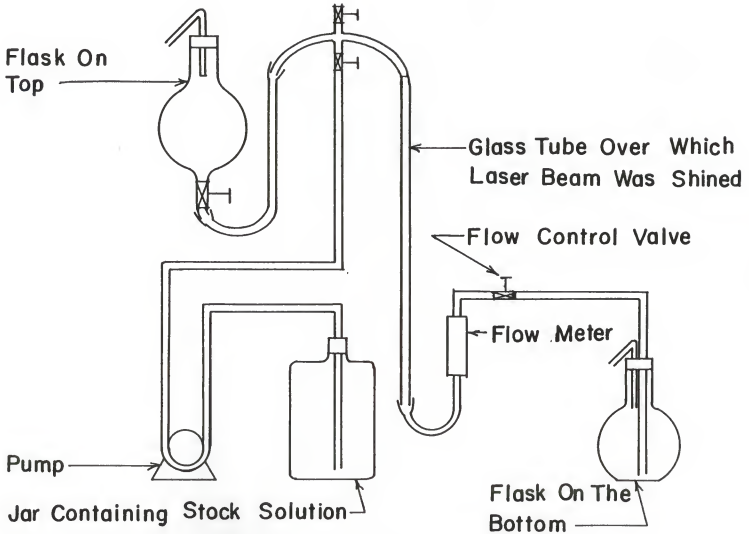
Flask On Top
Glass Tube Over Which Laser Beam Was Shined
Flow Control Valve
Flow Meter
Pump
Jar Containing Stock Solution
Flask On The Bottom

During the time the flow system was being made, we tried to study a system which didn't have Brownian motion, but had instead a pure translational motion. The correlation time for such a system is expected to be infinite and the beam transit time to be finite depending on the rate of translation. According to the plotting routine described in Section 3.2, the slope-intercept plot should give us a straight line passing through zero at zero time. Such a system is provided by a rotating ground glass. We could never see, however, the line going through zero, because of a dead-time problem in the pad.

The particles used to study the new flow system were 0.234 u in diameter and the concentration used was about 8.0×10^7 cm^{-3}. The water used in making the solution was filtered separately into a big jar and the polystyrene balls were suspended into the water. The whole flow system was cleaned and rinsed several times with filtered distilled water before introduction of the solution. Several different combinations of the optical settings were tried to see if we had any alignment problem. These were: 1) taking the PM tube close to the scattering volume and placing a pinhole in front, 2) taking the PM tube away from the scattering volume and focussing the beam from the tube to the slit right in front of the iris, and 3) the same as (2) but with the inclusion of a pinhole. The three different optical settings worked with didn't give us any difference in the results implying that there were not any coherence problems.

The data were taken at several different flowrates starting from zero up to a flow rate of 900 ml/min. The slope-intercept plot was made for each different flow. The Y-intercept was plotted against flow rate

as before. The plot was found to have a small positive slope for flow rates up to about 500 ml/min. From there up to 900 ml/min the plot was found to have a higher positive slope. So it seemed that there were two portions in the plot for which the flow behavior might be different. When we looked at the sample times used at different flow rates, however, it turned out that right after the flow of 500 ml/min, we had used smaller sample times for which the effects of afterpulsing may have been greater. As was mentioned before in the analysis of data, our procedure was to normalize the signal value with respect to that at the first or m^{th} channel and then proceeded further. If that value was in error, we were propagating the error throughout the analysis. Thus, we decided to fit the data directly to the correlation function. This reduced the afterpulsing problem, and we found that the data points for flows with afterpulsing came down and fell on the same line as with the others. The plot still has a small positive slope. The Y-intercept of the slope-intercept plot gives us information about diffusion, which becomes less and less contributing to the spectrum at higher flow rates where beam transit term dominates. We thought that this might be the reason for giving slightly higher values of the Y-intercept at higher flow rates. The size of the particles evaluated from the Y-intercept agreed well with the result from the static solution. The first and second cumulants came out reasonable. The S plot as was described in Section 3.2, was made out of the experimental data. It proved to be a nice straight line from where the beam width was calculated and subsequently from which the incident beam diameter was evaluated. We ran the experiment with three different lenses of three different focal length and made the S plot for each of them. The slopes scaled correctly with the focal length and the incident beam diameters calculated agreed well.

For smaller size particles the diffusion will be faster, the correlation time smaller, and consequently at a given flow rate the diffusion is expected to contribute relatively more to the spectrum than for larger particles. Thus if the small positive slope we found previously for 0.234 μ particles was due to the relative magnitudes of τ_1 and τ_2, the slope should go down for smaller particles like 0.091 μ. To see the effect we did a run on the 0.091 μ size particles and the slope did indeed prove to be smaller.

Next we tried to perturb the flow by hanging a small obstacle in the way of the flow from the top of the tube. The obstacle was very small in comparison to the tube diameter and it was about 3 ft. away from the scattering volume. We used 0.234 μ particles. We didn't see any change in the Y-intercept or slope in the slope-intercept plot from our nonperturbed flow with 0.234 μ size particles. We thought maybe the disturbance was not enough to give any appreciable effect. Afterwards we placed a much larger obstacle about ½ ft away from the scattering volume in the way of flow, and took data again. This time the Y-intercept started going up more and more with flow rate. The slope of the plot of Y-intercept against flow rate was about nine times higher than that without perturbation.

4.0 DISCUSSION AND CONCLUSION

The data taken after rebuilding the flow system are given in Tables 4.1 to 4.3, and the plots of the data are shown in Figs. 4.1 to 4.7. The particle size used first was nominally 0.234μ in diameter as given by the manufacturer, Dow Chemical Company. For these particles the average measured size of the particles came out to be 0.2294μ from the static data, which is only off by about -2.0%. This value is quite reasonable, considering possible errors incurred by uncertainties in temperature, which changes τ_1 by 3% for each °C, and uncertainty in scattering angle, which changes τ_1 by 1.7% at 90° if we are off the center line by about 0.5 mm. This result indicates that the controlling equation (Eq. 2.4.2.12) for the diffusional, no flow condition, holds. For the flowing system the slope-intercept plots were found to be straight lines indicating that the spectra was a product of an exponential and a Gaussian. For flowing systems, the plot of the Y-intercept of the slope-intercept plot against flow rate for particles of 0.234μ diameter is shown in Fig. 4.1. This plot rather than being flat as expected came out to have a small positive slope. The average size of the particles at a flow rate of 900 ml/min came out to be 0.164μ, which is off by -29.91%. At this flow rate, however, τ_2 is about 5 times faster than τ_1. The average size of the particles, using the average value of the Y-intercept obtained within the range of the experimental flow rates was 0.193 μ, which is off by about -17.50%. Once again, however, τ_2 is on the average about 4.5 times faster than τ_1.

Fig. 4.1 also shows the plot of the Y-intercept of the slope-intercept plot against flow rate for particles of 0.091 μ diameter. This plot indicates a small positive slope too, but the slope is smaller.

Table 4.1. Y-intercept and slope of the SI plot, τ_1 and τ_2 as a function of flow rate for particles of nominal diameter 0.234μ

Flow rate (ml/min)	Y-intercept x 10^{-3} (sec^{-1})	Slope x 10^{-7} (sec^{-2})	τ_1 x 10^4 (sec)	τ_2 x 10^4 (sec)
0	2.369	0	4.221	∞
50	2.320	.095	4.310	10.230
100	2.378	0.340	4.205	5.419
200	2.608	1.599	3.834	2.501
300	2.642	3.229	3.785	1.760
400	2.674	5.420	3.740	1.358
500	2.774	8.421	3.605	1.090
600	2.723	12.592	3.672	0.891
700	2.990	16.520	3.344	0.778
800	3.074	22.076	3.253	0.673
850	3.122	25.800	3.203	0.622
900	3.326	27.340	3.007	0.605

Table 4.2. Y-intercept and slope of the SI plot, τ_1 and τ_2 as a function of flow rate for particles of nominal diameter 0.091μ

Flow rate (ml/min)	Y-intercept x 10^{-3} (sec^{-1})	Slope x 10^{-7} (sec^{-2})	τ_1 x 10^4 (sec)	τ_2 x 10^4 (sec)
0	6.086	0	1.643	∞
100	6.144	0.217	1.627	6.789
200	6.120	1.218	1.634	2.865
400	6.142	4.080	1.628	1.565
500	6.211	6.588	1.610	1.232
600	6.426	9.609	1.556	1.020
700	6.416	13.076	1.558	0.874
800	6.446	17.891	1.551	0.747
900	6.488	22.226	1.541	0.671

Table 4.3. Y-intercept and slope of the SI plot as a function of flow rate for 3 focussing lenses of different focal lengths.

Focal Length, F = 15.3 cm

Flow rate (ml/min)	Y-intercept x 10^{-3} (sec^{-1})	Slope x 10^{-7} (sec^{-2})
0	6.385	0
100	6.551	0.679
200	6.967	3.594
400	7.817	11.135
600	9.132	28.062
800	10.571	49.106

Focal Length, F = 9.4 cm

Flow rate (ml/min)	Y-intercept x 10^{-3} (sec^{-1})	Slope x 10^{-7} (sec^{-2})
0	6.068	0
100	6.436	1.968
200	7.073	8.237
400	9.204	26.526

Focal Length, F = 30.0 cm

Flow rate (ml/min)	Y-intercept x 10^{-3}	Slope x 10^{-7}
0	6.160	0
100	6.225	0.129
200	6.331	0.765
400	6.412	2.685
600	7.333	5.646
800	7.653	10.371

Fig. 4.1. A graph of the Y-intercept of the SI plot against flow rate for particles of two different sizes.

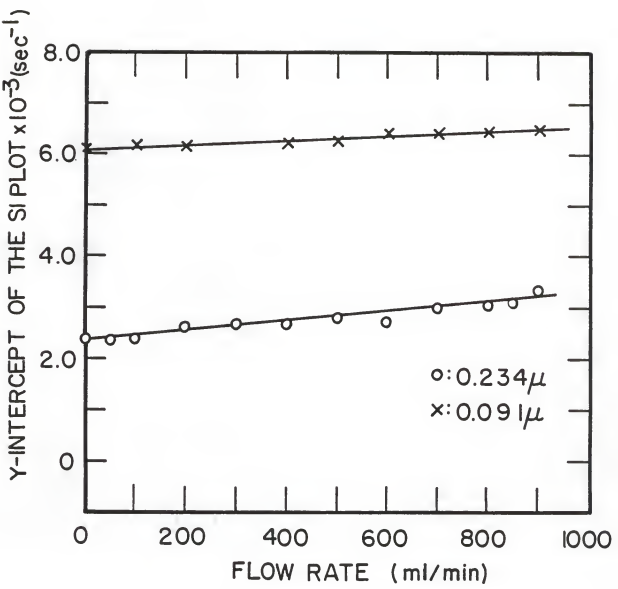
Y-INTERCEPT OF THE SI PLOT x10^{-3}(sec^{-1})
8.0
6.0
4.0
2.0
0
0
200
400
600
800
1000
FLOW RATE (ml/min)
o: 0.234μ
x: 0.091μ

The slope seems to scale with the particle size. The data for the no flow condition with these particles gave the average size of the particles as 0.0886 μ, which is off by -2.6% and which is, again in good agreement with the manufacturers value. At the flow rate of 900 ml/min the particle size turned out to be 0.0832 μ, which is off by -8.69%. The average value of the Y-intercept gave average particle size as 0.0858 μ, which is off by -5.7%. For these smaller particles, τ_2 is only 2.3 times faster than τ_1 at 900 ml/min. At the average value of the Y-intercept, the τ_2 is only 1.3 times faster than τ_1. At higher flow rates we still have the afterpulsing problem. Also the particles sweep by the scattering volume so fast that the diffusion may not contribute much information to the spectra for such a situation. This we think might be an important reason for the Y-intercept becoming larger at higher flow rates. The smaller particles diffuse faster than the bigger ones thus even at the same flow rate smaller particles should give more diffusional information than bigger ones. From the comparison of the graphs in Fig. 4.1, we really can see that the percentage increase of the Y-intercept for the smaller particles are much smaller than the bigger ones. So we conclude that the relative values of τ_1 and τ_2 are a determining factor for the behavior of the Y-intercept.

Figures 4.2 and 4.3 are plots of τ_1 and τ_2 against flow rates for 0.234 μ and 0.091μ particles, respectively. These plots indicate that we can separate τ_1 and τ_2 even when τ_2 is smaller than τ_1. This result was unexpected because it was felt that if $\tau_2 < \tau_1$ the quick decay of the Gaussian term would mask the decay of the exponential term which contains the useful diffusional information.

Fig. 4.2. A plot of τ_1 and τ_2 versus flow rate for particles of nominal diameter 0.234 μ.

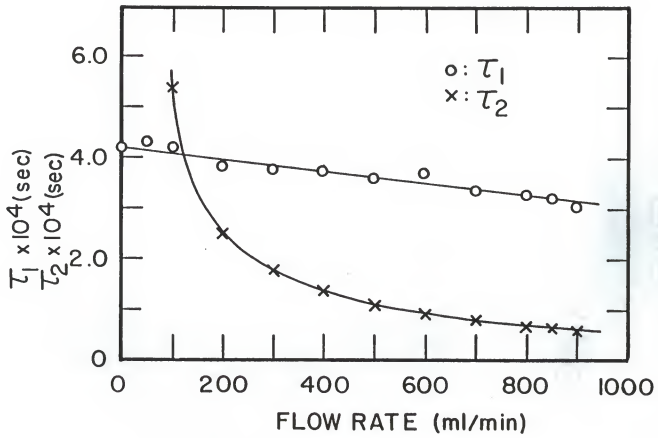
6.0
4.0
2.0
0
0
200
400
600
800
1000
o: τ_1
×: τ_2
$\tau_1 \times 10^4$(sec)
$\tau_2 \times 10^4$(sec)
FLOW RATE (ml/min)

Fig. 4.3. A plot of τ_1 and τ_2 versus flow rate for particles of nominal diameter 0.091 μ

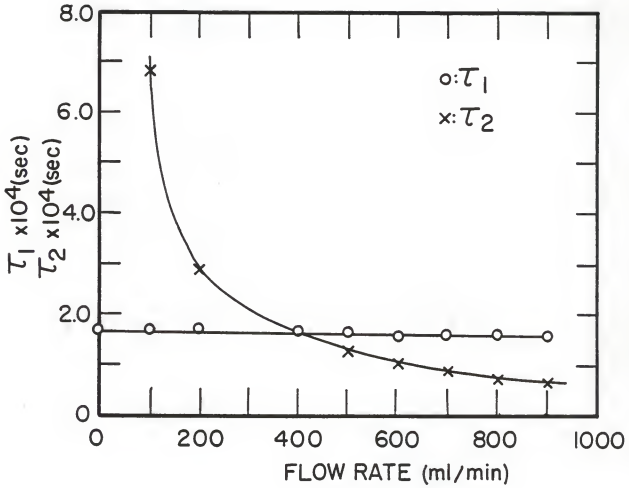
8.0
6.0
4.0
2.0
0
0
200
400
600
800
1000
o:τ1
x:τ2
τ1 x10⁴(sec)
τ2 x10⁴(sec)
FLOW RATE (ml/min)

Fig. 4.4, as described in Sec. 3.2, is an S plot. This, as we can see, is a straight line for both particle sizes. Fig. 4.5, is an S plot for 0.091 μ particle with three focussing lenses of different focal lengths, which corresponds to the data in Table 4.3. According to the plotting routine, the slope of these lines are $1/\tau_2^2$, which in turn is equal to $V^2/4\sigma^2$. So the slope of the S-plot should give σ, the beam width. Using diffraction theory, the incident beam diameter on the lenses was calculated. This diameter according to the theory is the diameter of the Gaussian beam for which the intensity is $1/e^2$ times that at the center of the beam. If 2W is this diameter, then

$$I = A_o^2 \, e^{-2r^2/W^2}.$$

In our derivation of correlation function we used

$$I = A_o^2 \, e^{-r^2/2\sigma^2}$$

so $W = 2\sigma$

According to the diffraction theory[7], the diameter of the incident beam 2W becomes

$$2W = \frac{4\lambda F}{\pi(2W_1)}$$

where, $2W_1$ is the diameter of the focussed beam which gives,

$$2W = \frac{\lambda F}{\pi\sigma}$$

For the three different lenses the incident beam diameters agreed to within 5%. The width of the beam for which the intensity is 1/e times that at the center was calculated too. The average width at $1/e^2$ point was found to be 0.35 cm, corresponding to 0.25 cm at the 1/e point. The

Fig. 4.4. A graph of the slope of the SI plot versus flow rate squared for particles of two different sizes.

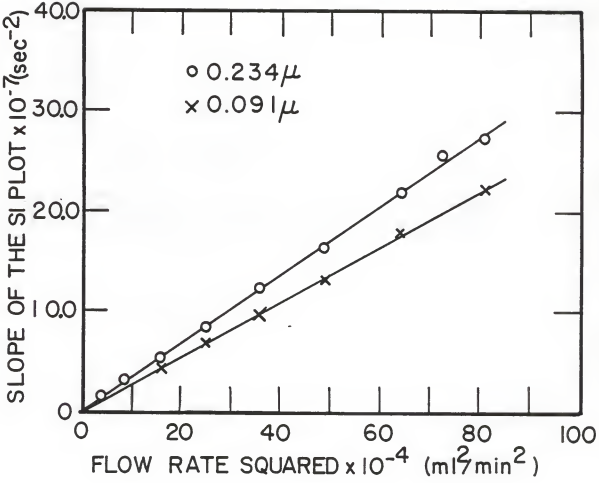
40.0
30.0
20.0
10.0
0
0.234μ
0.091μ
SLOPE OF THE SI PLOT x 10^-7 (sec^-2)
0
20
40
60
80
100
FLOW RATE SQUARED x 10^-4 (ml^2/min^2)

Fig. 4.5. A graph of the slope of the SI plot versus flow rate squared for three converging lenses of different focal lengths.

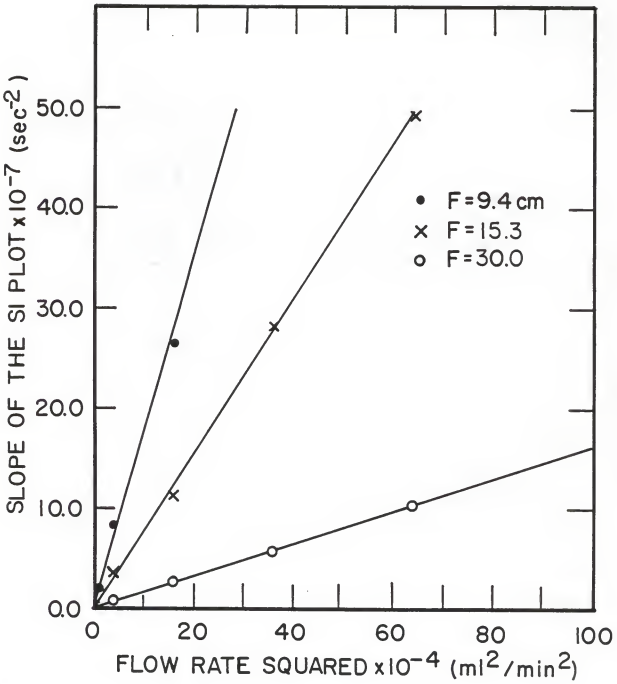
SLOPE OF THE SI PLOT x10^{-7} (sec^{-2})
50.0
40.0
30.0
20.0
10.0
0.0
0
20
40
60
80
100
FLOW RATE SQUARED x10^{-4} (ml^2/min^2)
F=9.4 cm
F=15.3
F=30.0

direct experimental measurement of the beam intensity with position in the beam is shown in Fig. 4.6. The measurement was done by placing a photomultiplier tube with a pinhole in front, perpendicular to the beam. The photomultiplier tube was mounted over a translator, which was graduated, so as to read the position of the tube within the beam. The PMT was connected to a photon counter. These data indicate that the actual beam widths at the $1/e^2$ and $1/e$ points were 0.293 cm and 0.195 cm, respectively. However, all these indicate that the controlling equation (Eq. 4.2.2.12) for the flowing particles works. So we can conclude that the light scattering by flowing and diffusing particles gave us information which agrees well with the theory.

When we were doing flow-experiments, we didn't really measure the aperture opening in the laser. But we adjusted the opening such that we were in the TEM_{oo} mode, for which the beam profile was Gaussian. This beam width varies with aperture opening and we weren't sure what the aperture opening was during the experiment. This may be a reason for which we found a difference between the calculated and measured beam diameters.

In Fig. 4.7, we see that for a highly perturbed flow, the Y-intercept shows a sharp rise with flow rate, which arises due to the disturbance within the flow. Turbulence in the flow is expected to increase the diffusion, which should give a high value of the first cumulant, i.e., a large Y-intercept. The same effect was observed in the perturbed flow. So we think that turbulence in the flow is causing it. We have not performed enough work on this phenomenum to give any positive remark.

Table 4.4. Intensity of the beam with position for about 80° aperature opening.

Position (cm)	Relative Intensity
2.30	0.20
2.32	0.20
2.36	0.40
2.38	0.65
2.40	1.15
2.42	1.70
2.44	2.60
2.46	4.05
2.48	4.85
2.50	6.05
2.52	6.60
2.54	6.60
2.56	6.35
2.58	5.40
2.60	3.90
2.62	2.70
2.64	2.05
2.66	1.45
2.68	1.00
2.70	0.55
2.72	0.30
2.74	0.15

Fig. 4.6. A plot of the beam profile for aperture opening of about 80°.

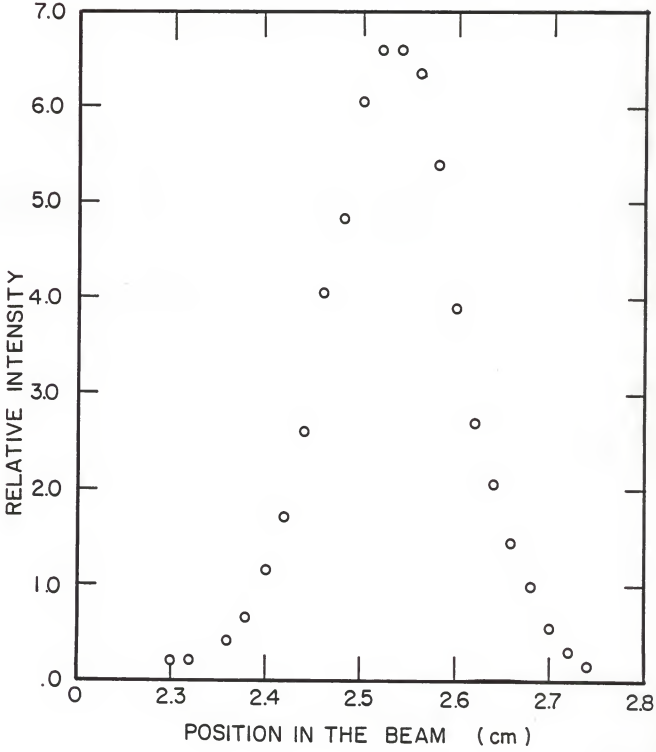
7.0
6.0
5.0
4.0
3.0
2.0
1.0
.0
RELATIVE INTENSITY
0
2.3
2.4
2.5
2.6
2.7
2.8
POSITION IN THE BEAM (cm)

Fig. 4.7. A graph of the Y-intercept of the SI plot versus flow-rate for highly perturbed flow.

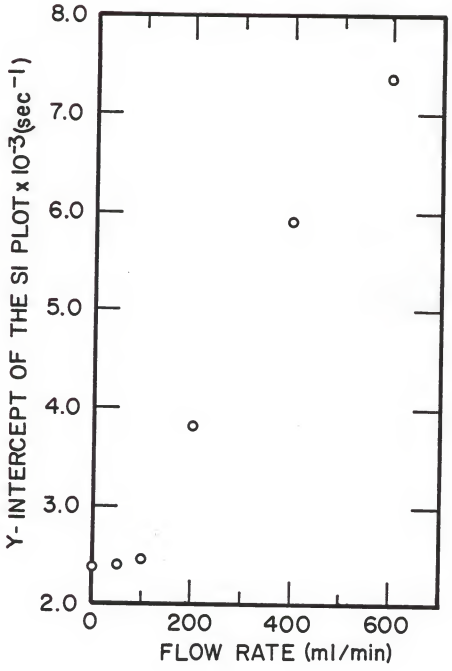
8.0
7.0
6.0
5.0
4.0
3.0
2.0
Y- INTERCEPT OF THE SI PLOT x 10⁻³(sec⁻¹)
0
200
400
600
FLOW RATE (ml/min)

In this thesis a theoretical expression was developed for the PCS spectrum of a system of diffusing and flowing particles. The theory was tested with a simple polystyrene-water system. The controlling equations for the two different conditions were found to work. The particle size measurements worked out in the no flow condition. The particle sizes agreed to within 3% of the manufacturers stated size. τ_1 and τ_2 were calculated for two different particle sizes at several different flow rates. For the smaller particles of 0.091 μ diameter τ_1 was found to be within 6% of its no flow value even at a very high flow of about 900 ml/min. For the bigger particles of 0.234 μ diameter the τ_1 at the flow rate of 900 ml/min was found to be within 30% of its no flow value. τ_1 and τ_2 were found to be separable at different flow rates. For a highly perturbed flow the measurements indicate that τ_1 even at 600 ml/min is about 70% off its true value. So turbulence in the flow is suspected to cause this big discrepancy. The beam width was calculated from τ_2 and also directly measured experimentally and the two agreed to within 15 to 20%. The method of analysis developed was found very useful and simple to use. This work can be used as an experimental basis for the future work with flowing Brownian motion systems.

REFERENCES

1. M. Kerker, The Scattering of Light and Other Electromagnetic Radiation, (Academic Press, New York, 1969).

2. B. J. Berne and R. Pecora, Dynamic Light Scattering, (John Wiley and Sons, New York, 1976).

3. B. Chu, Laser Light Scattering, (Academic Press, New York, 1974).

4. G. B. King, Ph.D. Thesis, Kansas State University, 1983.

5. E. R. Pike, Photon Correlation Spectroscopy and Velocimetry, edited by H. Z. Cummins and E. R. Pike, (Plenum Press, New York, 1977).

6. W. L. McCabe and J. C. Smith, Unit Operations of Chemical Engineering, (McGraw-Hill, Inc., Japan, 1976).

7. D. C. O'Shea, W. R. Callen and W. T. Rhodes, Introduction to Lasers and Their Applications, (Addison-Wesley Publishing Company, Inc., Philippines, 1977).

8. R. V. Edwards, J. C. Angus, M. J. French, and J. W. Dunning, Jr., J. App. Phys. 42, (2), 837, (1971).

9. C. M. Sorensen, R. C. Mockler, and W. J. O'Sullivan, Phys. Review, 17, (6), 2030, (1978).

10. L. E. Estes, L. M. Narducci, and R. A. Tuff, J. Optical Soc. of America, 61 (10), 1301, (1971).

11. I. J. Wygnanski, and F. H. Champagne, J. Fluid Mech., 59, (2) 281, (1973).

Acknowledgements

I would like to express my deep gratitude and sincere appreciation to Dr. Tom Taylor, Dr. Chris Sorensen, and Dr. Fred Merklin for their guidance and support throughout this study. Thanks is extended to Mr. Bill Starr for his assistance in repair of correlator and other equipment. I express my sincere appreciation to Dr. Tom Taylor for his help and for sharing his experience during the work. I acknowledge the help of Connie Schmidt for her excellent typing of this manuscript, and to Merna Brisbin for her assistance throughout my entire M.S. program. I acknowledge the friendship of those who extended their help whenever I needed. Finally, my deepest appreciation to my husband, Zahirul for his encouragement during this trying time.

APPLICATION OF PHOTON CORRELATION SPECTROSCOPY TO FLOWING BROWNIAN MOTION SYSTEMS

by

DALIA P. CHOWDHURY

B.S. Bangladesh University of Engineering and Technology, 1979

AN ABSTRACT OF A MASTER'S THESIS

Submitted in partial fulfillment of
the requirements for the degree

MASTER OF SCIENCE

College of Engineering
Department of Nuclear Engineering

KANSAS STATE UNIVERSITY

Manhattan, Kansas
1985

ABSTRACT

Flowing Brownian motion systems are encountered in many practical situations of interest e.g., soot particles in flames as well as other aerosol systems. Recently, the dynamic light scattering technique, Photon Correlation Spectroscopy (PCS) has proven useful for studying the diffusional processes in these aerosol systems. This has stimulated the need for an understanding of the PCS spectrum of such diffusing and flowing systems. A representative system of such a situation is polystyrene latex spheres suspended in water flowing through a tube at a known flow rate. Two terms 1) the correlation of time, τ_1, and 2) the beam transit term, τ_2, are useful in describing a system of particles which are diffusing while in bulk motion. τ_1 is due to the random Brownian diffusion of the particles while τ_2 arises due to the bulk motion of the particles with respect to the scattering volume. The diffusional term appears as an exponential and the beam transit term appears as a Gaussian in the correlation spectrum. A theoretical and experimental study of the PCS spectrum observed for light scattered from a flowing Brownian motion system was done. The study of the simple system allowed us to study the effect of both the diffusion and flow terms in the PCS spectrum and provided a testing ground for our theoretical understanding of the spectrum and the experimental technique. The theory works for such a system. Finally, it was found that τ_1 and τ_2 could be separated for different flow rates even when τ_2 was much faster than τ_1, a result not previously expected.